Solar Energy xxx (xxxx) 113521

Contents lists available at ScienceDirect

Solar Energy

journal homepage: www.elsevier.com/locate/solener

Tilted solar UV radiation estimation and its role in advanced solar water treatment systems

Lisdelys González-Rodríguez [a, b, *], Basharat Jamil [c], Mehmet Ali Kallioğlu [d], Alejandro Cabrera-Reina [e, g], Aitor Marzo [f, g], Wirmer García-Tuñon [h, i], Matías Volke [j], Fabiola Lobos [a, b], Agustin Laguarda [k]

[a] Centro de Modelación Ambiental y Dinámica de Sistemas (CEMADIS), Universidad de Las Américas, Santiago, Chile
[b] Facultad de Ingeniería y Negocios, Universidad de Las Américas, Sede Concepción, Concepción, Chile
[c] High Temperature Processes Unit, IMDEA Energy Institute, Av. Ramón de La Sagra, 3, Móstoles, 28935 Madrid, Spain
[d] Besiri OSB Vocational School, Batman University, 72060 Batman, Turkey
[e] Departamento de Ingeniería Química, Universidad de Almería, Ctra. Sacramento S/n, 04120 Almería, Spain
[f] Department of Optics, University of Granada, Profesor Adolfo Ranca¯no St, 18071, Granada, Spain.
[g] CIESOL, Joint Centre of the University of Almería-CIEMAT, 04120 Almería, Spain
[h] Programa de Doctorado en Ciencias con Mención en Biodiversidad y Biorecursos, Facultad de Ciencias, Universidad Católica de la Santísima Concepción, Concepción, Chile
[i] Data Observatory Foundation, ANID Technology Center No. DO210001, Santiago, Chile
[j] Facultad de Ingeniería, Universidad de Concepción, Concepción, Chile
[k] Laboratorio de Energía Solar, Facultad de Ingeniería, Universidad de la República (Udelar), Montevideo 11700, Uruguay

CORRECTED PROOF

ARTICLE INFO

Keywords:
Ultraviolet solar radiation
Solar spectral irradiance
Water treatment
Tilt angles
Empirical models
Chile

ABSTRACT

Information on solar ultraviolet radiation (UVR) on the Earth's surface is essential for fields such as health/materials sciences, and energy. UVR measurements are commonly taken on a horizontal plane, which is also the reference plane for the available database estimates. However, for many applications, such as water treatment, information on UVR in the tilted plane may provide more insightful results. There is a lack of studies in the literature that address the problem of UVR on inclined surfaces. In this study, an isotropic transposition model was used to estimate UVR in tilted surfaces in six different cities along the Chilean territory with potential applications in solar water treatment. In this context, isotropic refers to the diffuse and direct radiation component modeling. In addition, mathematical models were developed to forecast Chilean cities' monthly and yearly optimum tilt angles. The efficiency of the solar photo-Fenton process for treating paracetamol-contaminated wastewater using a compound parabolic collector photoreactor tilted at different angles, was evaluated through simulation. The gains increased at the highest latitude were 30.13 % for monthly, 21.05 % for seasonal, and 9.23 % for yearly adjustments. The empirical models developed were found to be highly accurate ($R^2 \geq 0.81$, RMSE $\leq 0.98°$, MAPE ≤ 2.70,% SSRE $\leq 0.01°$, RSE $\leq 0.02°$, and MBE $\leq 0.001°$). Using the local latitude as the photoreactor tilt angle (the current general design strategy) resulted in lower efficiency (m^3 of wastewater treated per month) than using the optimal tilt angle for the month with the lowest UVR (winter), and the entire year. These results highlight the importance of fine-tuning the photoreactor tilt angle locally and, consequently, the need to develop UVR models that account for this variable.

Nomenclature

Greek symbols

β	tilt angle of solar collector (°)
βopt	optimum tilt angle (°)
γ	surface azimuth angle (rad)
δ	declination (°)
θ	solar incidence angle (rad)
ρ	albedo of the ground
∅	latitude (rad)
ω	hour angle

* Corresponding author.
E-mail address: lgonzalezr@udla.cl (L. González-Rodríguez).

https://doi.org/10.1016/j.solener.2025.113521
Received 19 January 2025; Received in revised form 5 April 2025; Accepted 13 April 2025
0038-092/© 20XX

Note: Low-resolution images were used to create this PDF. The original images will be used in the final composition.

ΔE (%)	percentage gain in the availability of UVR_{β} on an inclined surface

Abbreviation

UVR_{g}	global solar ultraviolet radiation on a horizontal plane (Whm^{-2})
$UVR_{dir,\beta}$	direct or beam solar ultraviolet radiation on the inclined surface (Whm^{-2})
$UVR_{dif,\beta}$	diffuse solar ultraviolet radiation on the inclined surface (Whm^{-2})
$UVR_{r,\beta}$	solar ultraviolet radiation reflected by the ground (Whm^{-2})
UVR_{β}	total irradiance received on a tilted plane at an angle of inclination (Whm^{-2})
$UVR_{\beta opt}$	total irradiance received on the optimum angle of inclination (Whm^{-2})
$UVR_{\beta=0^{\circ}}$	solar ultraviolet radiation on a horizontal plane (Whm^{-2})
UVRb,n	direct solar ultraviolet radiation incident on a plane normal to the sun rays (Whm^{-2})
n	day of the year

1. Introduction

At present, the knowledge of ultraviolet solar radiation (UVR) is of great interest, as it has harmful effects on living beings [1], materials [2], and on the contrary, beneficial applications in different photochemical processes [3–5]. UVR corresponds to electromagnetic radiation emitted by the sun within the spectral range from 100 to 400 nm. It is subdivided into three spectral bands: UVR-C (100–280 nm), UVR-B (280–315 nm), and UVR-A (315–400 nm). UVR-C, which is toxic to life, is completely absorbed in the upper layers of the atmosphere by oxygen and ozone. Meanwhile, both UVR-B and UVR-A reach the Earth's surface. UVR-B is largely absorbed in the stratosphere by ozone, while both UV-B and UV-A are further attenuated by nitrated and aromatic aerosols, nitrated aromatic gases, and black carbon aerosol particles in polluted urban air [6]. From an energetic perspective, although UVR represents a relatively small fraction of the solar spectrum, at ground level around 5 % [7], its photons are highly energetic, even ionizing. Ionizing radiation has enough energy to remove tightly bound electrons from atoms, thus creating ions. This ionization process can lead to chemical reactions, which in biological systems can cause damage to cells and tissues. This property makes excessive exposure to UVR harmful to living organisms, causing issues like skin cancer, cataracts and pinguecula [1,8]. The exposure effect of UVR on human skin is usually based on ultraviolet erythemal radiation (UVER). The effect of UVR on human skin is often measured using ultraviolet erythemal radiation (UVER), which reflects skin sensitivity to different UVR wavelengths and is linked to indices like the UV index (UVI) [9].

In addition, UVR is a powerful disinfectant that can inactivate a wide range of harmful microorganisms in water [10–14]. Many studies have demonstrated the impact of UVR on various photocatalytic solar systems [2,15,16]. For instance, [16] compared the results of a study on solar water treatment efficiency (solar photo-Fenton) in three countries (Spain, Chile, and Qatar) concerning temperature and UVR resources. This demonstrated the importance of considering these factors in photoreactor design. Therefore, knowing the UVR resource is important for the design of solar photocatalytic systems that could be used in water detoxification/disinfection technologies.

In this context, the use of tilted photoreactors is a common practice. The tilting of photoreactors is often used to optimize solar radiation exposure, improve fluid dynamics and increase treatment efficiency. Tilting allows better alignment with the sun's rays [17–19] thus maximizing the activation of the photocatalysts and efficiency of photocatalytic reactions [20]. By optimizing sunlight exposure, photoreactors can operate more efficiently, potentially reducing the need for artificial light sources and saving energy. Furthermore, inclination facilitates oxygenation and prevents sedimentation of suspended particles, both of which are crucial for effective photocatalysis. Finally, it promotes efficient drainage, thus maintaining constant operation [21].

For the study of the UVR resource, the best accuracy is achieved with well-calibrated and well-maintained ground-based measurements made with UVR radiometers and spectroradiometers. Ground-based measurements are important for precise monitoring of incident UVR at a specific location, but they do not provide information on the UVR distribution for large areas. In addition, there is a lack of ground-based UVR databases due to the financial implications associated with the need to allocate space for instrument placement, and the acquisition, operation and maintenance costs of such equipment.

While less accurate, physical and mathematical models based on local atmospheric parameters for determining UVR levels offer a powerful alternative to ground-based measurements [22]. Physical and empirical models can be used to determine the UVR levels at different tilt angles. The tilt angle of a solar collector is the angle at which it is installed relative to the horizontal. The tilt angle can significantly affect the amount of solar radiation that a system receives, and thus the amount of UVR available for a specific process. This includes solar photoreactors used for solar water treatment, which consist of a recirculation tank connected to Pyrex glass tubes (through which water circulates) placed on the focus of compound parabolic collectors (usually known as CPCs).

Against this background, the estimation of the optimal tilt angle for solar photoreactors is key to the performance of solar water treatments. This should be discussed not only in terms of maximizing the energy received throughout the year but also considering the system's operability concerning local climate factors. Therefore, the availability of UVR data based on the tilt angle is essential for designing efficient solar water treatment systems that are adapted to treatment objectives and local conditions. Shukla and co-researchers presented a comparative evaluation of isotropic and anisotropic models for estimating monthly solar radiation over the entire spectral range on tilted surfaces oriented (tilt equal to the site latitude) to the Equator in Bhopal, India [23]. It was found that an isotropic model gave better estimates and reduced statistical errors. The Liu & Jordan model for inclined surfaces under isotropic atmospheric conditions and the HDKR model used for the evaluation of total solar radiation for inclined surfaces under anisotropic atmospheric conditions have been studied in [24]. Subsequently, Maleki et al. showed that among isotropic models the most accurate is the Liu-Jordan model [25]. Following similar lines, the research reported by [26] for the estimation of UVER on several planes also concluded that the isotropic model does not present significant differences compared to the rest of the models despite using fewer parameters. The isotropic model employs the most straightforward representation of diffuse radiation, assuming its homogenous distribution across the sky [23]. This assumption is particularly valid in the UVR spectral range, as several studies have shown that diffuse sky radiance tends to be more isotropic in the UVR than at longer wavelengths. This is mainly due to Rayleigh scattering, which dominates in the UVR and exhibits an almost isotropic spatial distribution, unlike aerosol scattering, which is highly anisotropic and becomes more relevant at longer wavelengths [27–29]. Conversely, as UVR undergoes the significant scattering in the Earth's atmosphere, attributing an isotropic character to solar radiation in this spectral range is a valid approximation.

The estimation of the tilt angle using modelling has been conducted by numerous researchers in countries such as India [23,30], the United Arab Emirates [31,32], España [26,33], Turkey [34,35], Saudi Arabia

UNCORRECTED PROOF

[36,37], Africa [38], Brazil [39], India [24] and Chile [40]. In contrast to the UVR spectral range, there is an abundance of databases on solar global irradiance at different tilt angles in the visible and near-infrared, due to the proliferation of solar energy plants. In general terms, an orientation towards the Equator and a fixed tilt angle of β (tilt) = φ (latitude) is usually recommended [41] which yields acceptable accuracy [42,43], but the optimal tilt angle is also influenced by the local climate which is why it is not always equal to the latitude [44]. Generalized rules of thumb, such as setting the tilt equal to latitude or adjusting by ± 10-20°, may not always be accurate. Kallioğlu et al. [35] mentioned that for Muğla (37.20° N-28.37° E), Turkey found the best annual angle was 32.25°. Therefore, on occasion, the tilt angle could be different in some grades to latitude. Another study mentioned the optimization of solar panel angles for maximum solar efficiency. Ref [18] focused on the impact of solar panel angles on productivity in Belgrade, Serbia. They found that adjusting the tilt angle could lead to significant increases in productivity, ranging from 5.98 % annually to 15.42 % monthly. Related to the UVR band, some authors such as [26] and [45,46] modeled UVER on inclined planes and demonstrated that the intensity of UVR at different inclination angles is different.

Serrano et al. [47] estimated the UVI for two tilted planes with different orientations. They concluded that their approach provided a good estimate of the UVI, compared to experimental values, in 99 % of cases. Other research [33] analyzed four years of solar UVR measurements performed on tilted and horizontal planes at Plataforma Solar de Almería, Spain, for solar water treatment. The authors demonstrated that a photoreactor tilted to 37° (local latitude) and facing south will receive annually about 3–4 % more UVR energy than a horizontal plane. However, they also showed that the optimal tilt angle varies between 14° (June) and 60° (December), suggesting a monthly tilt adjustment to maximize the UVR exposure of the water treatment system.

In developing countries such as Chile, access to clean water can be a challenge, especially in arid and semi-arid areas. Furthermore, several studies have recognized contamination in various surface water bodies throughout the country [48–50]. Given the importance of UVR in water treatment and the geographical diversity of Chile, it is crucial to research UVR resources and the optimal tilt angle for solar applications. In Chile, the estimation or measurement of solar radiation, which is essential for UVR water treatment, is typically done on a horizontal plane [9,51,52]. However, few studies have reported UVR on inclined surfaces. In addition, there is limited work in determining the optimum angle of inclination to improve the UVR gains in solar water collectors. The country's diverse geography, ranging from the Atacama Desert in the north to the extended forests and lakes in the south, offers a wide range of solar radiation conditions that can be used to develop new models to estimate the optimal tilt angle for solar collectors. This will not only improve the efficiency of solar water treatment systems, but it will also contribute to the country's sustainable development goals.

In this context, this study aims to address the following research question: What is the optimal tilt angle that maximizes UVR capture in solar photoreactors for water treatment in different regions of Chile? Furthermore, can empirical models be developed to estimate this angle based on local climate variables?

This research is based on the hypothesis that the optimal tilt angle for solar photoreactors does not necessarily coincide with the site's latitude and that empirical models can provide a more accurate estimation by accounting for geographical and seasonal variability.

Under this general perspective, the objectives of this study include (i) to determine the monthly, seasonal, and yearly optimum tilt angles and UVR energy gains in different cities of Chile and (ii) to develop empirical models to calculate the monthly and annual optimum tilt angle for any Chilean region, and (iii) to explore the implication of the tilt angle of photoreactors on the operational flexibility and efficiency of solar water treatments. This paper analyses the potential of solar UVR for the integration of water treatment technologies in Chilean cities (located between −18.44°S and −41.41°S latitude), considering different installation configurations to improve their efficiency (UVR energy gains). The optimization of tilt angle in solar photoreactors represents a novel and significant contribution to the field of solar energy utilization. Some novel contributions are: (1) By optimizing the tilt angle, solar photoreactors can maximize the capture of UVR, which is crucial for effective water treatment processes. This enhancement in energy capture directly translates to improved system efficiency and performance. (2) The ability to adjust the tilt angle dynamically allows solar photoreactors to adapt to changing environmental conditions, such as monthly/seasonal variations in solar declination and local weather patterns. This adaptability ensures consistent system performance and reliability. (3) By maximizing solar radiation capture, optimized tilt angles reduce the need for auxiliary energy inputs, thereby increasing the overall energy efficiency of the system. This efficiency gain is particularly important in regions with limited solar resources. (4) By enhancing the performance of solar water treatment systems, optimized tilt angles contribute to environmental sustainability. These systems offer a renewable and clean energy solution for water treatment, reducing reliance on fossil fuels and minimizing environmental impact. So, by enhancing energy capture, improving system efficiency, and promoting sustainability, optimized tilt angles offer a promising pathway for advancing solar water treatment technologies. Continued research and innovation in this area hold the potential to drive further advancements and broaden the impact of solar photoreactors in addressing global water treatment challenges.

2. Materials and methods

This section is devoted to a detailed exposition of the fundamental elements and procedures that were utilised in the course of the research.

2.1. Locations of study

Chile is located between 17° 30′ and 56° 30′ South latitude and occupies a long coastal strip between the Andes mountains and the Pacific Ocean in the southwestern part of South America (Fig. 1a). Throughout the year, the territory receives a good amount of solar radiation, especially in the Northern regions (Atacama Desert). Generally, Chile receives from the Sun between 900–2200 kWh/m^2 annually [31] For this study, 6 Chilean communities between 18°S and 41°S South latitudes were selected. From north to south: (Fig. 1b) Arica, (Fig. 1c) Antofagasta, (Fig. 1d) Santiago, (Fig. 1e) Concepcion, (Fig. 1f) Temuco, and (Fig. 1g) Puerto Montt. The criteria for selecting the locations were based on adequate spacing to cover a range of latitudes including populated areas with industrial and economic activities with different energy needs in terms of access, costs, and demand. In addition, it captured the climate variations throughout the territory. Table 1 shows the exact location of the Chilean cities, population, and climate types.

2.2. Databases

The Angström Beta parameter, and Water Vapour (WV, cm) and radiometric UVR data were obtained from SoDa Services (https://www.soda-pro.com/soda-products) [53,54]. This service delivers typical values for UVR-A and UVR-B based on climatological data under all sky conditions [53]. The UVR data are derived from the HelioClim-1 and HelioClim-2 satellite databases, with HelioClim-1 covering the period 1985–2005 and HelioClim-2 providing data from February 2004 onwards. The dataset has been validated through comparisons with ground-based measurements from the Baseline Surface Radiation Network (BSRN) and meteorological networks of the World Meteorological Organization (WMO)] [55–57]. UVR values are available at monthly, daily, and hourly resolutions, with a spatial resolution of approximately

CORRECTED PROOF

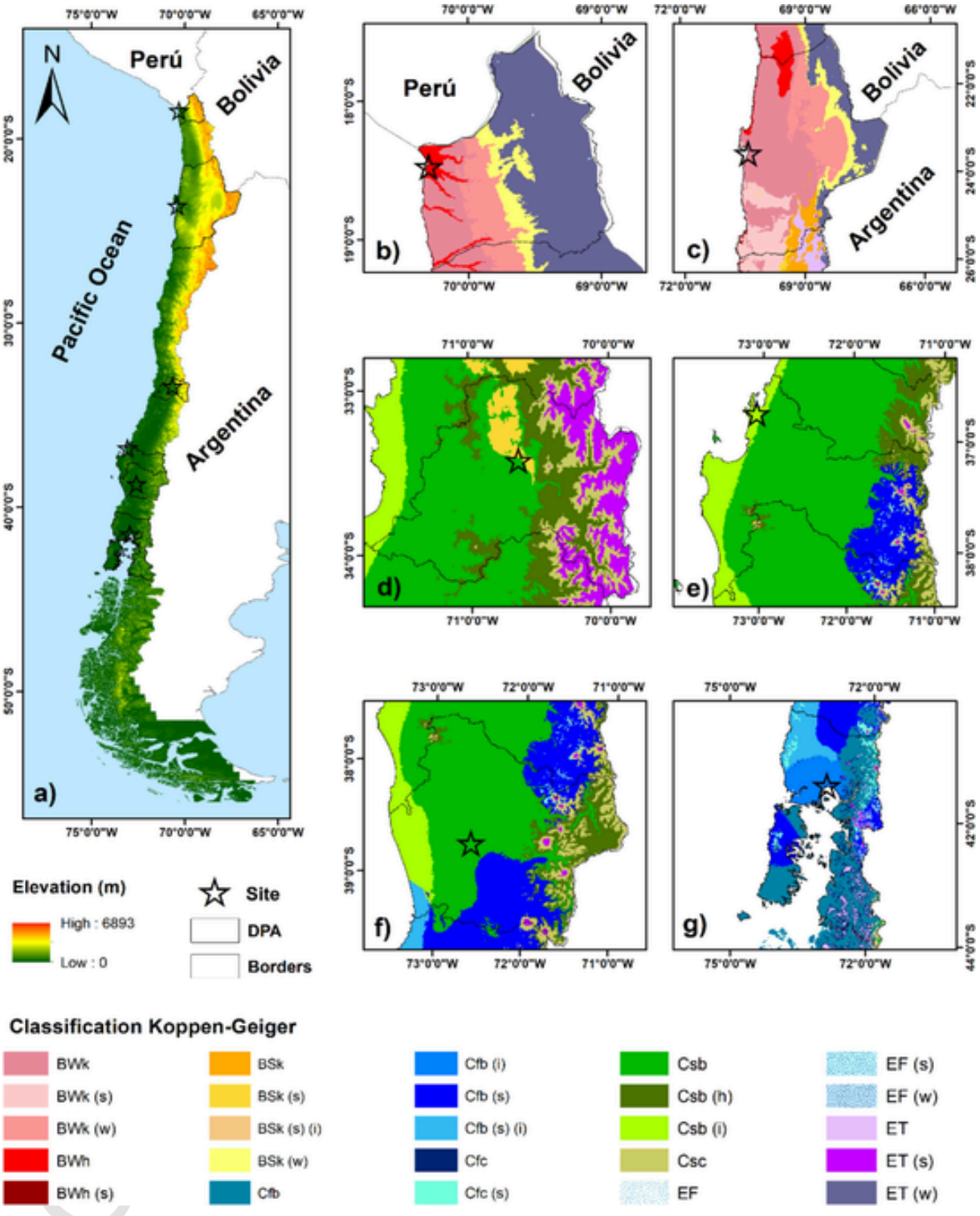

Fig. 1. (a) Location of Chile in South America with topographic profile, zoom of sites selected (b) Arica, (c) Antofagasta, (d) Santiago, (e) Concepcion, (f) Temuco and (g) Puerto Montt. A star represents the location. The shapefiles were obtained from the Ministry of National Assets, Geospatial Data Infrastructure (IDE, http://www.ide.cl/).

50×50 km^2 for daily irradiance data prior to 2004. This service delivers typical values for UVR-A and UVR-B based on climatological data (1961–1990) under all sky conditions [41]. A typical mean year was used, which is relevant since the data have considerable inter-annual UVR variability. This UVR dataset has been used by other researchers to estimate UVR daily doses [58], and testing and validation of the new solar models [59]. Then, the sum of UVR-A and UVR-B bands over a horizontal plane for six Chilean cities with different climatological conditions was calculated. The stratospheric ozone concentration in Dobson Units (DU) during the 1960–2020 period was obtained from NASA (https://ozonewatch.gsfc.nasa.gov/). Clouds are one of the major modulators of UVR, especially in mid-latitude. For that, the cloud frequency

Table 1
Features of the study locations.

Site	Latitude (ϕ°S)	Longitude (°W)	Altitude (m.a.s.l)	Climate type[a]	Region	Population[b] (hab)
Arica	−18.44	−70.21	5	Cold/Hot desert	Arica-Parinacota	226,068
Antofagasta	−23.59	−70.39	150		Antofagasta	607,534
Santiago	−33.49	−70.73	500	Mediterranean	Metropolitan	7, 112.808
Concepcion	−36.73	−72.46	121		Biobío	2,037.414
Temuco	−38.68	−72.60	360		Araucania	957,224
Puerto Montt	−41.41	−72.92	105	Temperate rainy	Los Lagos	828,708

[a] Köppen-Geiger climate classification
[b] hab «Plantilla Censo 2017».

is estimated as the ratio of the number of cloudy bins to the total bins scanned by CloudSat Calipso (Cloud–Aerosol Lidar and Infrared Pathfinder Satellite Observations) satellite considering a period of observation from 1983 to 2015 [60]. The lidar is near-nadir pointing and provides measurements at a vertical resolution of 60 m and a horizontal resolution of 330 m. CALIPSO orbits Earth about 16 times a day and a near-global coverage of 82°N–82°S [61].

2.3. UVR modeling on tilted surfaces and gains

The estimation of incident UVR on tilted surfaces is necessary to optimize the efficient use of the incoming radiation. The amount of solar energy received on a surface depends on the local sky conditions, but also on the latitude (φ), the day of the year (n), the tilt angle (β), the azimuth angle of the surface (γ), the time during the day (hour angle, ω), and the solar incidence angle of the radiarion beam (θ). By optimizing the configuration factors, of the photoreactor, the amount of UVR energy received on their surface can be maximized thereby improving the efficiency of solar energy systems. Usually, global UVR (UVRg, in Wh/m^2) is measured or estimated in a horizontal plane. To convert UVRg to different tilt angles the methodology for broadband radiation described in [31] was used. The total irradiance received on a plane with given tilt (β) and azimuth (γ) angles, can be expressed as the sum of three terms: UVR direct ($^{UVR}_{dir,\beta}$), diffuse UVR ($^{UVR}_{dif,\beta}$) and reflected UVR by the ground ($^{UVR}_{r,\beta}$), in the absence of nearby bodies:

$$UVR_{\beta,\gamma} = UVR_{dir,\beta,\gamma} + UVR_{dif,\beta,\gamma} + UVR_{r,\beta,\gamma} \quad (1)$$

The first term, corresponding to the direct UVR, is given by the geometric relationship:

$$UVR_{dir,\beta} = UVR_{b,n}\cos\theta \quad (2)$$

where, $^{UVR}_{b,n}$ is the direct UVR incident on a plane normal to the sun rays, and theta (θ) is the angle between the direct beam of the sun and the normal to the tilted plane of interest.. On the other hand, if the albedo is considered isotropic on a tilted plane [62], the $^{UVR}_{dif,\beta}$ and $^{UVR}_{r,\beta}$ are calculated as:

$$UVR_{dif,\beta} = \frac{1}{2}\rho \cdot UVR_g\,(1+\cos\beta) \quad (3a)$$

$$UVR_{r,\beta} = \frac{1}{2}\rho \cdot UVR_g\,(1-\cos\beta) \quad (3b)$$

where, $^{UVR}_{g}$ is the global UVR received on a horizontal plane and ρ is the ground albedo that in this work has a constant value of 0.2. The monthly, season and annual UVR received by a fixed surface with different tilts and orientations (β and γ, respectively) were calculated for each site selected. To have enough data to allow an accurate chart, the following scheme was conceived: The orientation corresponds to the azimuthal angle starting from the cardinal point north (180°) and increasing clockwise from 30° in steps of 30°. The tilt angle was positioned from completely horizontal (0°) to completely vertical (90°) and calculated every 1°. The figures were generated using the graphic software OriginPro 2023b (64-bit) SR110.0.5.157 (Academic). The percentage gain (ΔE,%) on a monthly, seasonal and annual basis was calculated using Equation 4 [30]. Relating the availability of $^{UVR}_{\beta}$ on an optimally inclined surface compared to the horizontal surface [30]

$$\Delta E\,(\%) = \left(\frac{\left.\frac{UVR}{\beta}\right|_{\beta=\beta opt_i}}{\left.\frac{UVR}{\beta}\right|_{\beta=0^\circ}} - 1 \right) \times 100 \quad (4)$$

where i = monthly, seasonal, and annual

2.4. Correlation functions

To calculate the average optimal slope angle according to latitude and UVR data 15 empirical models were adjusted developed. They are related to the optimization of the tilt angle for the harvesting of higher UVR energy in several Chilean latitudes. The correlation functions developed were subjected to statistical analysis. Seven different statistical indicators were used, coefficient of determination (R^2), mean absolute error percentage (MAPE, %), sum square relative error (SSRE, degree), relative standard error (RSE, degree), mean bias error (MBE, degree), relative error (RE, degree) and root mean bias error (RMSE, degree) [63]. Equations 5–11 represent the statistical indicators used.

$$R^2 = \left(\frac{\sum_{i=1}^{n}\left(O_i-\overline{O}\right)\left(P_i-\overline{P}\right)}{\sqrt{\sum_{i=1}^{n}\left(O_i-\overline{O}\right)^2\sum_{i=1}^{n}\left(P_i-\overline{P}\right)^2}} \right)^2 \quad (5)$$

$$MAPE = \frac{100}{n}\sum_{i=1}^{n}\left|\frac{O_i-P_i}{O_i}\right| \quad (6)$$

$$SSRE = \sum_{i=1}^{n}\left(\frac{O_i-P_i}{O_i}\right)^2 \quad (7)$$

$$RSE = \sqrt{\frac{\sum_{i=1}^{n}\left(\frac{O_i-P_i}{O_i}\right)^2}{n}} \quad (8)$$

$$MBE = \frac{1}{n}\sum_{i=1}^{n}\left(P_i-O_i\right) \quad (9)$$

$$RE = \left(\frac{O_i-P_i}{O_i}\right) \text{ x } 100 \quad (10)$$

$$RMSE = \sqrt{\frac{1}{n}\sum_{i=1}^{n}\left(P_i-O_i\right)^2} \quad (11)$$

Where Pi and Oi represent the modeled and observed values, n represents the number of observations and $\overline{O}$ is the arithmetic mean of the observations. The results obtained were compared with previous studies developed in the Southern Hemisphere.

CORRECTED PROOF

2.5. Kinetic model

The photo-Fenton kinetic model was originally developed by Cabrera-Reina et al. [64]. It is based on the reactions and mass balances of the most relevant components of the process, and has been used for simulating solar wastewater treatment. With temperature and UVR (ambient conditions) as inputs, this model can predict the treatment time ($t_{treatment}$) required to achieve a specific decontamination level. Thus, since this work focuses on developing an empirical model for predicting UVR at different tilt angles, the newly available data will enable the kinetic model to evaluate the impact of the photoreactor's tilt angle on treatment efficiency. Although changes in the system's tilt angle do not affect acquisition costs, selecting an appropriate tilt angle can enhance the treatment efficiency and potentially reduce operational and total costs. Additionally, available temperature records can be incorporated into the model to adjust the kinetic constants of the reactions, following Arrhenius-type equations. The significant impact of temperature on photo-Fenton process efficiency is well-known: in general, increasing the operational temperature raises the kinetic constants and, consequently, the reaction rates [65]. However, there is an upper temperature threshold beyond which iron precipitation is favored, leading to reduced treatment efficiency [66]. Fortunately, this threshold is typically well above ambient temperatures. This study chose wastewater contaminated with paracetamol at a concentration of 100 mg L^{-1} total organic carbon (TOC) as the model wastewater. The target mineralization level was set at 75 %, and the daily treatment volume was 100 m^3. UVR data from the previous modelling was used, while temperature data was obtained from [64]. Once the treatment time under the corresponding ambient conditions is determined by simulation, the number of batches ($N_{batches}$) that can be processed within a given period is calculated by dividing the number of sun hours for this period (W) by the treatment time. Finally, the photoreactor size can be determined by dividing the volume of wastewater to be treated during this period by the number of batches that can be processed. Treatment capacity (TC), defined as the volume of water that can be treated per month or year, can be obtained by multiplying the photoreactor volume by the number of batches that can be carried out during the corresponding period.

$$N_{batches} = \frac{W}{t_{treatment}} \tag{12}$$

$$V_{photoreactor} = \frac{V_{objective}}{N_{batches}} \tag{13}$$

$$TC = N_{batches} \cdot V_{photoreactor} \tag{14}$$

3. Results and discussion

3.1. Atmospheric parameters

UVR values depend on local atmospheric and weather conditions, making it crucial to study the specific characteristics of the location of interest. Fig. 2 illustrates the resulting values of the beta Angstrom parameter (beta, without units), stratospheric ozone content (in Dobson Units, DU), and water vapor (WV, in cm) for the study sites: Arica,

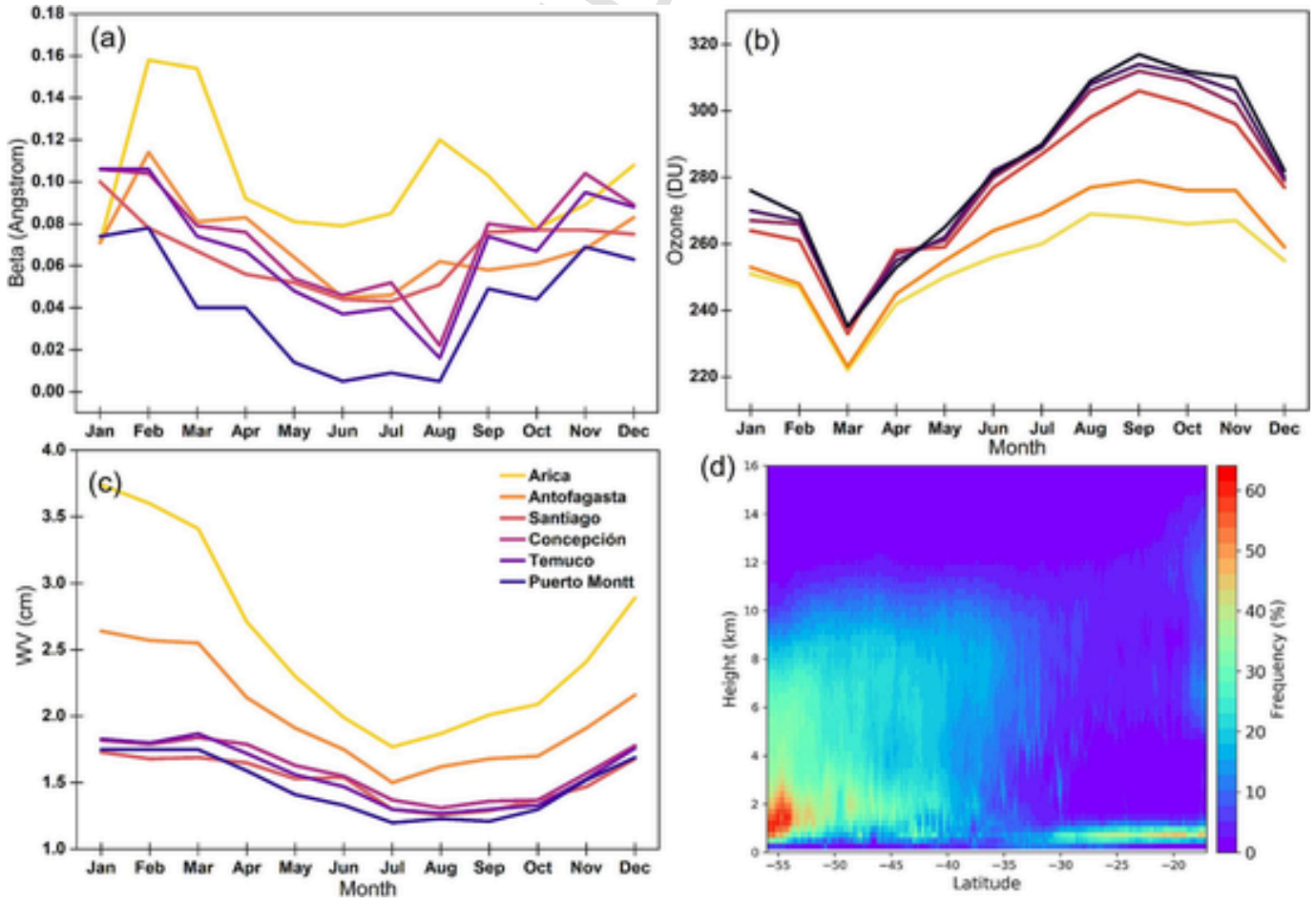

Fig. 2. Climatological values of (a) Beta, (b) Stratospheric ozone content, (c) Water vapour, and (d) Cloud frequency including height in km for each location under study.

Antofagasta, Santiago, Concepción, Temuco, and Puerto Montt. It also shows the frequency of cloud occurrence, including height in km, as a function of latitude from 15°S to 55°S. Please note that the range of latitudes considered in this study is from −18.5° in Arica to −41.41° in Puerto Mont. As illustrated in Fig. 2d, there is a marked increase in the presence of clouds south of −30°. This coincides with the boundary of the Atacama Desert. Below −30°, the frequency of occurrence of cirrus, cirrostratus, and cirrocumulus above 5 km increases. Their presence is approximately 35 %. The presence of clouds increases for more southerly latitudes, as well as their occurrence at lower altitudes. It should be noted that stratus, stratocumulus, and cumulus clouds form below 2 km with a frequency of occurrence of more than 60 % at latitudes around 55°S. However, this latitude corresponds to the Magallanes and Antarctic region, which is outside the scope of this study.

As illustrated in Fig. 2d, the Atacama Desert, located north of −30° latitude, experiences a scarcity of clouds, except for formations below one kilometer. These clouds are of the stratus and stratocumulus variety and are formed in the coastal zone. The orography of the Atacama Desert in Chile coastal mountains at west and Andes mountains at the east, acts as a climatic screen, preventing these types of clouds from passing into the interior of the desert [67]. The coastal and Andes Mountain ranges exert a significant influence on the low cloud presence and high solar resource of the Atacama Desert, with an annual solar resource of over 2500 kW h/m^2 [68]. The values of the Angstrom beta, ozone, and water vapor parameters shown in Fig. 2 a, b, and c, respectively, demonstrate seasonal behavior. In general, stratospheric ozone levels (Fig. 2 b) are lower in the northernmost locations, especially in Arica and Antofagasta, located in the Atacama Desert, with a minimum of 220 DU. This corresponds to higher levels of UVR. These values increase during the spring months and exceed 315 DU at sites in Concepción, Temuco, and Puerto Montt. Atmospheric turbidity, indicated by the values of the Angstrom beta parameter (Fig. 2a), shows its minimum values in winter, close to 0, with the highest values always for the localities of the Atacama Desert, reaching values of 0.16 in Arica in summer. The atmospheric water content has maximum values in summer, 3.6 cm and 2.6 cm for Arica and Antofagasta, respectively. It shows its minimum values in winter, reaching 1.2 cm for Puerto Montt in July.

3.2. Monthly horizontal analysis

Selecting North-facing for all cities, the $^{UVR}_{\beta=0^\circ}$ values in Whm^{-2} per month under all sky conditions on the horizontal surface ($\beta = 0^\circ$) were calculated. This data can be used as a baseline to compare UVR values on tilted surfaces. Table 2 shows the data of UVR obtained. It is seen that the summer season (Dec, Jan, Feb) in Arica receives a huge amount of UVR with a maximum value observed in January (436 Whm^{-2} month). The minimum values are reported in the winter season (Jun, Jul, Aug) in Temuco obtained in June/July (68.78 Whm^{-2} month). Arica, which likely has a location closer to the equator receives a high amount of UVR. This makes sense as the sun is at its highest point in the sky during these months, leading to more direct sunlight and thus more UVR. In the south-central regions of Chile, such as Santiago and Concepcion, UVR levels can also be high (411.00 and 417.51 Whm^{-2} month), especially during the summer months. However, during the winter months, UVR levels are usually lower for Puerto Montt (70.47 Whm^{-2} month) and Temuco (68.78 Whm^{-2} month). The factors presented in section 3.1 stratospheric ozone, clouds, and latitude determine the spatial–temporal distribution of UVR at the surface, and the results presented here are influenced by these factors.

3.3. Optimum monthly, seasonal, and annual tilt angles

Table 3 and Fig. 3 shows the monthly, seasonal, and annual optimum tilt angles for the selected locations. The optimum angle varies depending on the geographical location and the time of year. In Chile, these adjustments are significant due to the country's wide range of latitudes. The data from Chilean cities shows that the optimum tilt angle is different across the country. In the southern cities, the sun is lower in the sky and the days are shorter in winter, which means that a steeper tilt angle is needed to capture as much sunlight as possible. This is reflected in the data, which shows higher optimum tilt angles in the southern cities during the winter months. Monthly optimum angles in winter months ranged from 30°-38° (Arica) to 35°-44° (Puerto Montt). The annual optimum angle for each city was 25° (Arica), 27° (Antofagasta), 29° (Santiago), 30° (Concepcion), 28° (Temuco), and 31° (Puerto Montt). Interestingly, the data suggests that in the northern cities of Chile, the annual optimal tilt angle is close to the local latitude − 4°, as seen in Antofagasta. However, in the southern cities, the difference between the optimal tilt angle and the latitude increases, with Puerto Montt showing a difference of + 10°. This could be due to the increased incidence of cloud cover and lower solar radiation levels in the southern regions.

3.4. Monthly, season and yearly UVR values using optimum tilt angles and gains

Table 4 shows the UVR estimated for NW-facing surfaces using monthly, seasonal, and annual optimum tilt angles. After analyzing the results, it is evident that adjusting the solar collector tilt angles based on the specific month, season, and yearly can optimize the benefits of UVR. The values of UVR at monthly, seasonal, and annual using optimum tilt angles were observed to be maximum from October to February for all cities. These months correspond to the spring and summer seasons in the Southern Hemisphere when the sun is at its highest point in the sky and solar radiation is at its maximum. The city of Arica presented the highest monthly, seasonal and annual maximum values of UVR, corresponding to 447.45 Whm^{-2}, 430.86 Whm^{-2} and 357.62 Whm^{-2}, using what is considered to be the optimum tilt angle for January, Summer and yearly. The lowest maximum monthly UVR values of 82.69 Whm^{-2} and 91.71 Whm^{-2} (June month) were estimated for Temuco and Puerto Montt. If considering fixed yearly optimum tilt angle the maximum values of UVR with fixed yearly optimum tilt angle were observed in Arica (356.85 Whm^{-2}), Antofagasta (327.32 Whm^{-2}), Concepción (265.91 Whm^{-2}) and Santiago (264.41Whm^{-2}-), with the lowest value observed in Temuco (273.91Whm^{-2}-month) and Puerto

Table 2
Monthly $^{UVR}_{\beta=0^\circ}$ values in Whm^{-2} under all sky conditions in the horizontal surface at North-facing.

Cities	Month											
	Dec	Jan	Feb	Mar	Apr	May	Jun	Jul	Aug	Sep	Oct	Nov
Arica	428.74	436.13	407.04	360.70	328.11	235.91	206.41	210.54	251.02	314.60	389.71	435.78
Antofagasta	418.36	415.72	374.25	353.22	260.95	198.30	176.22	183.76	223.18	281.76	353.07	405.84
Santiago	411.00	411.73	354.07	284.82	196.15	115.20	77.94	95.64	135.37	172.68	291.19	373.45
Concepcion	417.51	415.51	345.69	281.73	182.41	104.25	82.06	86.49	136.06	211.63	304.05	364.38
Temuco	366.50	378.93	352.82	265.34	158.98	89.68	68.78	74.44	115.96	176.48	264.23	314.93
Puerto Montt	366.84	348.97	299.95	234.39	151.66	84.19	70.47	74.87	116.57	180.27	262.90	316.74

CORRECTED PROOF

Table 3
Monthly, seasonal, and annual optimum tilt angles for the selected locations.

Cities	Months											
	Dec	Jan	Feb	Mar	Apr	May	Jun	Jul	Aug	Sep	Oct	Nov
Arica	8°	14°	18°	28°	30°	33°	38°	34°	30°	27°	21°	14°
Antofagasta	16°	14°	19°	27°	30°	39°	40°	38°	31°	28°	22°	14°
Santiago	21°	22°	31°	35°	37°	37°	36°	35°	30°	24°	21°	19°
Concepcion	22°	24°	30°	37°	38°	37°	38°	36°	31°	24°	21°	21°
Temuco	22°	24°	31°	34°	32°	31°	30°	33°	29°	24°	22°	21°
Puerto Montt	21°	22°	24°	33°	37°	39°	44°	42°	35°	33°	24°	22°
Seasons												
	Summer			**Autumn**			**Winter**			**Spring**		
Arica	14°			29°			34°			21°		
Antofagasta	14°			31°			36°			21°		
Santiago	14°			31°			36°			21°		
Concepcion	21°			33°			36°			24°		
Temuco	21°			33°			36°			24°		
Puerto Montt	22°			35°			40°			24°		
Annually												
Arica	25°											
Antofagasta	27°											
Santiago	29°											
Concepcion	30°											
Temuco	28°											
Puerto Montt	31°											

Montt (227.82 Whm^{-2}). This discrepancy may be attributed to the varying geographical locations and climatic conditions of these cities (see Fig. 2). Additionally, the findings indicate that the estimated annual average UVR at the optimal seasonal and annual tilt angles is lower than the estimated annual average UVR at the optimal monthly tilt angle. This implies that adjusting the tilt angle of solar panels on a monthly basis could potentially enhance the UVR harvest.

Table 5 shows the percentage change (ΔE, %) upon monthly, season, and yearly tilt adjustments. It is evident from the results shown in Table 5 that the monthly adjusted tilt angle provides the highest average energy gain followed by the seasonal adjustments. The study also found that the yearly tilt adjustment provided the least amount of energy gain. This is because the yearly tilt adjustment does not consider the changes in solar radiation throughout the year, leading to less efficient use of solar energy. The percentage gain in annual average total UVR on monthly optimum tilt angle in comparison to a horizontal surface ranged between 1.83 %-30.13 % for Arica and Puerto Montt. This is due to the large diffuse component in the UVR range, a product of large Rayleigh scattering and aerosol absorption. It is therefore recommended that, whenever possible, the tilt angle of the solar photoreactors should be adjusted according to the monthly or seasonal tilt angles to make the best use of the available solar energy. This recommendation is further substantiated by the findings of [33].

3.5. Correlation functions

Twelve mathematical relations have been developed to provide the monthly optimum panel tilt angle specific to the Chilean territory. The optimum tilt angle (βopt.) is obtained from the relationships between latitude and UVR. This functional dependency is usually best expressed by multivariate non-linear equations [69]. The equation developed analyses two independent variables in the form of quadratic nonlinear regression equation. Different correlation functions were derived by applying multiple regression analysis to obtain a regression plane for the two-dimensional case. As illustrated in Fig. 4, the monthly correlation graphs of the models developed for the estimation of the monthly panel tilt angle for Chilean territory are displayed. The sharp transitions in

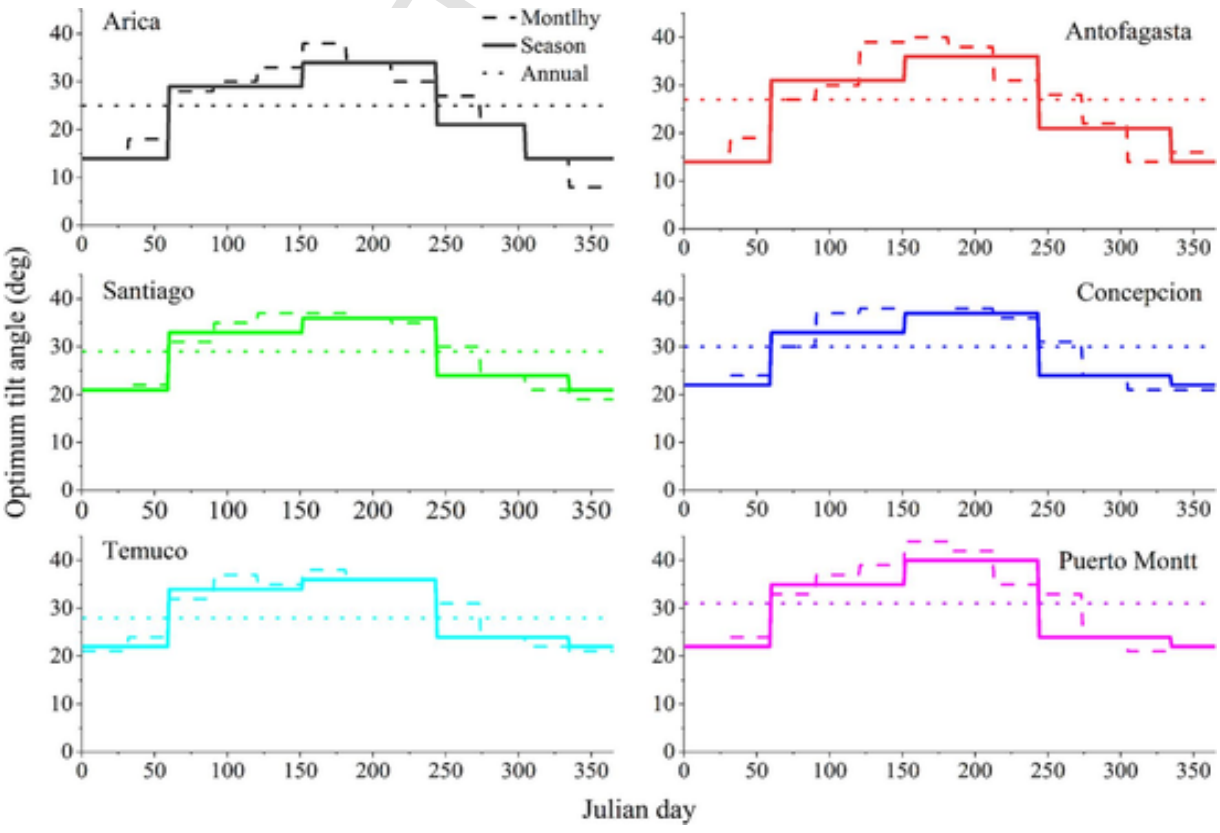

Fig. 3. Variations of monthly, seasonal, and annual optimum tilt angles for North-facing at different Chilean latitudes.

Table 4
Total UVR values in Whm^{-2} for North-facing surfaces at monthly, seasonal, and annual optimum tilt angles.

	Arica			Antofagasta			Santiago		
	Monthly	**Seasonal**	**Annual**	**Monthly**	**Seasonal**	**Annual**	**Monthly**	**Seasonal**	**Annual**
Dec	5.51	433.42	356.85	432.63	423.09	327.32	429.08	414.81	264.41
Jan	447.45			435.57			434.67		
Feb	421.92			392.37			377.02		
Mar	394.39	385.07		386.20	306.25		320.88	229.45	
Apr	379.79			298.15			229.59		
May	273.36			236.65			137.90		
Jun	241.71	255.59		211.08	226.67		95.38	121.77	
Jul	242.34			215.60			114.15		
Aug	286.19			253.89			154.95		
Sep	344.29	424.03		314.07	368.25		194.65	206.53	
Oct	408.33			372.35			312.65		
Nov	443.74			424.49			395.21		
	Concepción			**Temuco**			**Puerto Montt**		
	Monthly	**Seasonal**	**Annual**	**Monthly**	**Seasonal**	**Annual**	**Monthly**	**Seasonal**	**Annual**
Dec	434.69	418.77	265.91	378.99	388.13	273.91	381.85	359.24	227.82
Jan	439.62			399.65			365.86		
Feb	378.04			385.48			326.89		
Mar	314.96	219.17		300.82	198.11		265.79	182.13	
Apr	215.58			186.50			177.64		
May	126.85			106.64			102.83		
Jun	97.18	119.70		82.69	102.06		91.71	106.84	
Jul	104.01			89.49			94.40		
Aug	157.19			133.37			133.91		
Sep	237.01	317.07		196.70	271.36		206.02	274.78	
Oct	329.70			285.01			286.03		
Nov	384.09			331.90			331.93		

Table 5
The percentage change (ΔE, %) upon monthly, season, and annual tilt adjusted.

	Arica			Antofagasta			Santiago		
	Monthly	**Seasonal**	**Annual**	**Monthly**	**Seasonal**	**Annual**	**Monthly**	**Seasonal**	**Annual**
Dec	3.91	2.09	7.08	3.41	5.04	7.89	4.40	5.40	8.91
Jan	2.60			4.78			5.57		
Feb	3.66			4.81			6.48		
Mar	9.11	11.72		9.33	13.08		12.66	15.45	
Apr	15.75			14.26			17.05		
May	15.87			18.83			19.70		
Jun	17.10	14.70		19.78	16.60		22.38	17.94	
Jul	15.11			19.78			19.36		
Aug	14.01			13.76			14.46		
Sep	9.44	2.83		11.47	6.33		12.72	10.65	
Oct	4.78			5.46			7.37		
Nov	1.83			4.61			5.83		
	Concepción			**Temuco**			**Puerto Montt**		
	Monthly	**Seasonal**	**Annual**	**Monthly**	**Seasonal**	**Annual**	**Monthly**	**Seasonal**	**Annual**
Dec	4.12	6.16	9.04	3.41	5.89	9.01	4.09	5.70	9.23
Jan	5.80			5.47			4.84		
Feb	9.36			9.25			8.98		
Mar	11.79	15.63		13.37	15.54		13.40	16.15	
Apr	18.18			17.31			17.13		
May	21.69			18.91			22.14		
Jun	18.42	17.64		20.21	17.87		30.13	22.12	
Jul	20.26			20.22			26.09		
Aug	15.53			15.01			14.88		
Sep	11.99	8.04		11.46	7.67		14.28	8.43	
Oct	8.44			7.86			8.79		
Nov	5.41			5.39			4.79		

the graph are due to the sudden changes in the optimum tilt angle in the geographical region where the calculations are made. Specifically, fluctuations in the optimum panel tilt angle at certain latitudes can be attributed to solar declination and the regional distribution of solar radiation, which is contingent on atmospheric conditions. The analyses conducted permit the estimation of the monthly optimum tilt angle between latitudes −18.44°S and −41.41°S. It is important to note that the validity of these results extends to all the regions that have been studied..

The second-order multiple quadratic equations developed for January to December are shown below respectively.

$$\beta_{OPT.} = -861.6 - 10.77\,(\phi) + 3.311\,(\mathrm{UVR}) - 0.01898\,(\phi)^2 - 0.003097\,(\mathrm{UVR})^2 + 0.02133\,(\phi) \times \mathrm{UVR} \quad (14)$$

CORRECTED PROOF

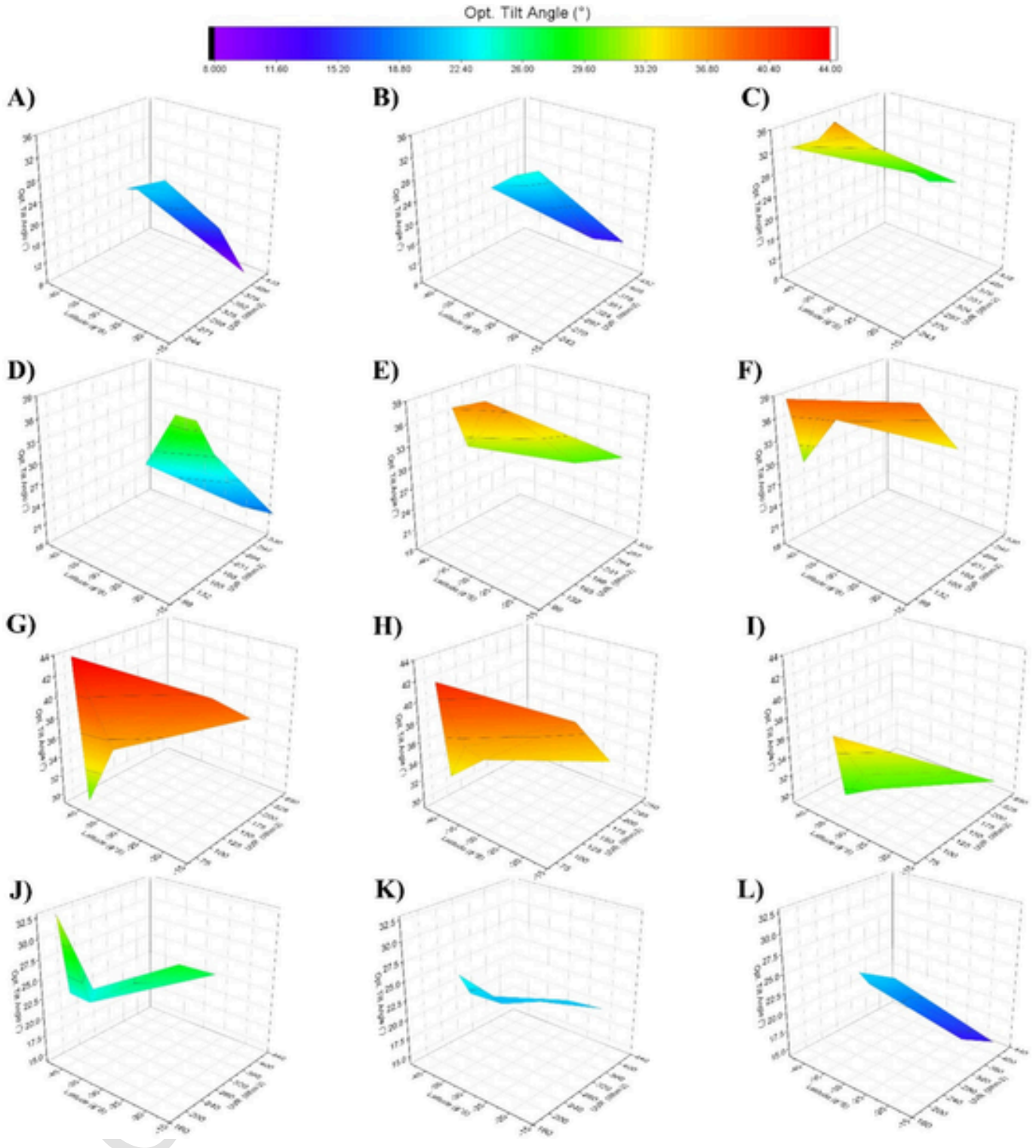

Fig. 4. Correlation functions provide monthly optimum tilt angles for Chilean territory. a) December, b) January, c) February, d) March, e) April, f) May, g) June, h) July, i) August, j) September, k) October, and l) November.

$$\beta_{OPT.} = 34.66 - 11.60\,(\phi) - 1.471\,(\mathrm{UVR}) - 0.1302\,(\phi)^2 + 0.002762\,(\mathrm{UVR})^2 + 0.006037\,(\phi) \times \mathrm{UVR} \quad (15)$$

$$\beta_{OPT.} = 6467 + 154.1\,(\phi) - 26.54\,(\mathrm{UVR}) + 0.9011\,(\phi)^2 + 0.02706\,(\mathrm{UVR})^2 - 0.3234\,(\phi) \times \mathrm{UVR} \quad (16)$$

$$\beta_{OPT.} = 4351 + 146.4\,(\phi) - 19.37\,(\mathrm{UVR}) + 1.225\,(\phi)^2 + 0.02137\,(\mathrm{UVR})^2 - 0.3335\,(\phi) \times (\mathrm{UVR}) \quad (17)$$

$$\beta_{OPT.} = 19526 + 698.1\,(\phi) - 130.6\,(\mathrm{UVR}) + 6.182\,(\phi)^2 + 0.2102\,(\mathrm{UVR})^2 - 2.387\,(\phi) \times (\mathrm{UVR}) \quad (18)$$

$$\beta_{OPT.} = 331.9 + 30.02(\phi) + 5.143(UVR) + 0.4607(\phi)^2 - 0.01941(UVR)^2 + 0.03451(\phi) \times (UVR) \quad (19)$$

$$\beta_{OPT.} = -46.41 + 4.460(\phi) + 2.211(UVR) + 0.1076(\phi)^2 - 0.006516(UVR)^2 + 0.01306(\phi) \times (UVR) \quad (20)$$

$$\beta_{OPT.} = 1222 + 44.68(\phi) - 6.166(UVR) + 0.4151(\phi)^2 + 0.007921(UVR)^2 - 0.1166(\phi) \times UVR \quad (21)$$

$$\beta_{OPT.} = -52.29 + 26.54(\phi) + 5.823(UVR) + 0.4055(\phi)^2 - 0.01309(UVR)^2 + 0.01812(\phi) \times (UVR) \quad (22)$$

$$\beta_{OPT.} = -10881 - 266.4(\phi) + 41.84\,UVR - 1.659(\phi)^2 - 0.04033(UVR)^2 + 0.5048(\phi) \times (UVR) \quad (23)$$

$$\beta_{OPT.} = -125.0 - 6.672(\phi) + 0.07195(UVR) - 0.04613(\phi)^2 + 0.000343(UVR)^2 + 0.008186(\phi) \times (UVR) \quad (24)$$

$$\beta_{OPT.} = -209.1 + 22.44(\phi) + 3.326(UVR) + 0.07374(\phi)^2 - 0.006352(UVR)^2 - 0.04396(\phi) \times (UVR) \quad (25)$$

In this study, statistical methods were employed to examine the relationship between the prediction results of the models developed for the Chilean region and the calculated values, which were derived from satellite data. This analysis aimed to assess the accuracy and reliability of the models by comparing their outputs with empirically obtained values, thereby providing a comprehensive evaluation of their predictive performance. As demonstrated in Table 6, all models exhibit R^2 values that are closely approximately by 1 signifyng a high degree of compatibility. Conversely, the remaining statistical methods demonstrate a proximity to 0, indicating that they are generally at statistically acceptable levels.. The best and the worst monthly prediction models were found for July-Eq.20 and May-Eq.18, respectively.

Table 7 shows that all models have a high predictive power when analyzed regionally. Temuco (−38.68° S) has the closest results to the calculated values with an error rate of 1.26 %, while Antofagasta (–23.59° S) has the worst representativeness with an average of 3.97 %. However, the annual average relative error rates for all regions are less than 5 %, which is ideal.

There is limited work in the Southern Hemisphere to statistically compare monthly values. However, the optimal annual tilt angle value can be obtained by comparing other models in the literature. Then, to generalize the results, correlations have been formulated for the annual optimum tilt angle in the six Chilean communities under study. Annual optimum tilt angles can be represented as a function of the latitude as shown in Fig. 5. Equations 26 to 28 represent linear, second-degree polynomial (quadratic) and third-degree polynomial (cubic) mathematical models, respectively.

$$\beta_{OPT.} = -1.2404(\phi) + 20.473 \quad (26)$$

$$\beta_{OPT.} = 0.0024(\phi)^2 + 0.3844(\phi) + 18.512 \quad (27)$$

$$\beta_{OPT.} = -0.0011(\phi)^3 - 0.101(\phi)^2 - 3.2647(\phi) + 8.1762 \quad (28)$$

Using these mathematical models, it is possible to determine the optimum tilt angle on an annual basis.

The mathematical models have been verified using various statistical tools and the results are presented in Table 8. Equation 28 provides the most appropriate results in terms of R^2 with a value of 0.8308. Equations 26 and 27 follow with lower R^2 values, respectively. The values of other statistical results are close to zero and at reasonable desirable levels.

Several equations have been developed in the literature to determine the optimal tilt angle for solar panels based on latitude [35,42,70]. The purpose of these equations is to calculate the annual average optimal angle according to latitude data. Table 9 compares previous studies in the Southern Hemisphere with the values obtained in the current study. Table 9 shows that the difference between the current study's yearly optimum tilt angle and the reference values is insignificant. The smallest deviation between the developed models and the reference values was found in South Africa (Pretoria) with 0.18° using the quadratic model, while the largest deviation was found in Brazil (São Paulo) with 10.06° using the cubic model. Therefore, when comparing the models developed with the previous reference values, the deviation was within an acceptable range for all regions.

3.6. The influence of photoreactor tilt angle selection in solar water treatments

In the field of solar water treatment, the most extended system is the tubular photoreactor including CPCs. These systems are often designed with the CPC's fixed tilt angle equal to local latitude, to maximize the solar radiation captured for extended periods of operation. While this design strategy is widely accepted and supported by scientific evidence, as extensively described in [74], this study presents new data that allows for a more comprehensive analysis.

The challenge of scaling up photoreactors has previously been addressed through simulation using kinetic models in which UVR and temperature data as model input [5]. This helps predict process efficiency in terms of treatment time, reagent consumption, and other key factors [64]. Selecting the appropriate photoreactor size to treat a daily volume of wastewater is challenging, as it depends on solar radiation availability, which fluctuates significantly throughout the year [16]. Although the system design can be based on the average annual UVR value, this approach results in an oversized photoreactor for the spring/summer months when more wastewater can be treated, and an undersized one for the autumn/winter months, leading to untreated wastewater accumulation until the sunnier periods return. Alternatively, a more conservative scale-up strategy involves designing the photoreactor based on the lowest UVR month. While this simplifies plant operation – since only cloudy or rainy days would disrupt the process – it also significantly increases the process costs, as the required photoreactor size would be much larger (higher acquisition costs).

The use of UVR estimation models capable of predicting UVR at different tilt angles offers a powerful tool for optimizing photoreactor design on a local scale. Rather than using the local latitude as a fixed tilt angle for solar CPC photoreactors, adjusting the tilt to the optimal angle for months or seasons with lower UVR levels could improve treatment efficiency during less favourable conditions. Although this approach may slightly reduce efficiency during periods with the highest UVR, it can help maintain more consistent treatment capacity, minimizing fluctuations that could negatively affect the scale-up process of photoreactors. In this context, four design alternatives for tilt angles are analyzed using Arica city as an example: (i) the optimal tilt angle for June, the month with the lowest average UVR of the year, (ii) the optimal tilt an-

Table 6
The outcome of the statistical indicators of the monthly mathematical models developed to estimate the optimal angle.

Statical Analysis	Eq.14	Eq.15	Eq.16	Eq.17	Eq.18	Eq.19	Eq.20	Eq.21	Eq.22	Eq.23	Eq.24	Eq.25
R^2	0.9802	0.9956	0.9702	0.9801	0.9901	0.9945	0.9902	0.9976	0.9908	0.9924	0.9951	0.9911
MAPE	0.4165	0.3272	4.4092	1.8291	6.2816	0.3740	0.2100	0.9869	0.7483	3.9913	0.2030	0.9457
SSRE	0.0001	0.0001	0.0427	0.0021	0.0935	0.0001	0.0001	0.0006	0.0005	0.0127	0.0001	0.0006
RSE	0.0030	0.0032	0.0597	0.0134	0.0883	0.0028	0.0015	0.0070	0.0063	0.0325	0.0017	0.0068
MBE	0.0839	0.0555	−2.6938	−0.6106	4.4754	−0.1407	0.0758	−0.3051	−0.2010	0.8859	−0.0324	−0.1659
RMSE	0.0868	0.0866	2.6963	0.6212	4.5151	0.1505	0.0773	0.3054	0.2430	1.0586	0.0356	0.1702

CORRECTED PROOF

Table 7
Relative error (%) and predicted monthly optimum tilt angles of the developed equations for six Chilean regions.

Cities	Months																					
	Jan		Feb		Mar		Apr		May		Jun		Jul		Aug		Sep		Oct		Nov		Dec	
	RE	P	RE	P	RE	P	RE	P	RE	P	RE	P	RE	P	RE	P	RE	P	RE	P	RE	P	RE	P
Arica	0.3	14.0°	0.9	17.8°	8.9	30.5°	2.8	30.8°	16.6	27.5°	0.6	38.2°	0.3	33.9°	1.0	30.3°	1.6	27.4°	4.4	20.1°	6.7	13.1°	1.3	8.1°
Antofagasta	0.4	13.9°	0.6	18.9°	9.7	29.6°	8.9	32.7°	18.3	31.9°	0.5	40.2°	0.2	37.9°	0.9	31.3°	1.2	28.3°	5.9	20.7°	0.3	14.0°	0.8	16.1°
Santiago	0.4	21.9°	0.2	31.0°	7.7	37.7°	3.9	35.6°	8.5	33.9°	0.3	36.1°	0.2	34.9°	1.0	30.3°	0.4	24.1°	0.0	21.0°	0.2	19.0°	0.8	21.2°
Concepcion	0.4	23.9°	0.1	30.0°	7.5	39.8°	1.5	38.6°	7.1	34.4°	0.3	38.1°	0.2	35.9°	1.0	31.3°	4.8	25.2°	1.6	21.3°	4.6	20.0°	1.4	21.7°
Temuco	0.4	23.9°	0.1	31.0°	8.2	36.8°	1.6	32.5°	0.2	31.0°	0.3	30.1°	0.2	32.9°	1.1	29.3°	0.4	24.1°	1.7	21.6°	0.1	21.0°	0.9	22.2°
Puerto Montt	0.5	21.9°	0.2	24.0°	8.5	35.8°	1.4	37.5°	10.3	35.0°	0.2	44.1°	0.2	41.9°	0.9	35.3°	0.3	33.1°	6.4	22.5°	0.1	22.0°	1.0	21.2°

P: Predicted monthly optimum tilt angles.

CORRECTED PROOF

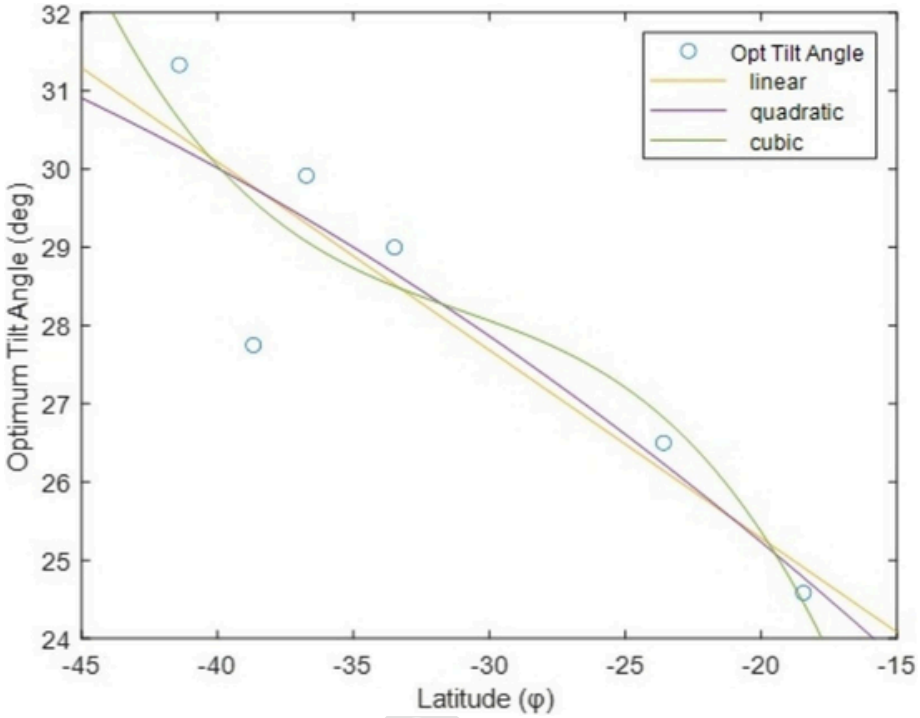

Fig. 5. Correlation functions provide annual optimum tilt angles for for Chilean territory (latitudes between −18.44°S to −41.41°S). Yellow, purple and green lines represent linear, quadratic and cubic correlation functions.. (For interpretation of the references to colour in this figure legend, the reader is referred to the web version of this article.)

Table 8
Statistical analysis of the developed annual mathematical models.

Statistical Indicators	Eq.26	Eq.27	Eq.28
R^2	0.8059	0.8083	0.8308
MAPE	2.6977	2.4735	2.3957
SSRE	0.0066	0.0064	0.0098
RSE	0.0234	0.0231	0.0286
MBE	−0.0011	0.0228	0.7220
RMSE	0.9782	0.9723	1.2342

gle for the entire winter period, (iii) the optimal tilt angle for the entire year, and (iv) the tilt angle corresponding to the local latitude (18°S), which serves as the baseline for comparison, reflecting the current design strategy. The treatment time required to achieve a 75 % reduction in the initial TOC concentration of paracetamol-contaminated wastewater under the four design alternatives described above was obtained through simulation using the corresponding monthly UVR and temperature average values, as outlined in Section 2.4.

The monthly variation in treatment time throughout the year is shown in Fig. 6. As expected, regardless of the selected design strategy, the treatment time fluctuates throughout the year, increasing during the winter months and decreasing during the summer months. The results indicate that using the local latitude as the tilt angle leads to the

Table 9
Optimum tilt angle reported by previous studies and current research for South latitudes.

Location				**Previous Study**		**Developed Models**			**Previous Model**		
Country	City	Lat.	Long.	Reference	β_{opt}°	Linear	Quadratic	Cubic	[42]	[71]	[35]
Brazil	Brasilia	−15.78	−47.89	[72]	20.00	24.27	23.98	22.51	17.72	17.94	12.37
Chile	Arica	−18.44	−70.21	**Present Study**	25.00	24.91	24.78	24.58	19.82	19.75	14.72
Brasil	São Paulo	−23.54	−46.65	[72]	17.00	26.13	26.23	27.06	23.40	23.22	19.23
Chile	Antofagasta	−23.59	−70.39	**Present Study**	27.00	26.14	26.24	27.07	22.00	23.25	19.27
South Africa	Pretoria	−25.74	28.18	[70]	27.00	26.66	26.82	27.70	24.80	24.72	21.18
Australia	Brisbane	−27.40	153.02	[73]	26.00	27.06	27.24	28.08	25.80	25.85	22.64
South Africa	Vryheid	−27.82	30.49	[70]	29.00	27.16	27.35	28.16	26.05	26.13	23.02
	Richtersveld	−28.56	16.76		26.00	27.34	27.53	28.31	26.48	26.64	23.67
	Bloemfontein	−29.11	26.18		28.00	27.47	27.67	28.41	26.80	27.01	24.16
	Durban	−29.87	30.97		29.00	27.65	27.85	28.54	27.24	27.53	24.83
	Van Rhynsdorp	−31.61	18.73		27.00	28.07	28.26	28.85	28.22	28.71	26.37
	Graaff-Reinet	−32.48	24.58		29.00	28.28	28.47	29.00	28.70	29.30	27.14
Chile	Santiago	−33.49	−70.73	**Present Study**	29.00	28.52	28.69	29.20	29.25	29.99	28.03
South Africa	Stellenbosch	−33.92	18.86	[70]	27.00	28.63	28.79	29.29	29.48	30.28	28.41
Chile	Concepcion	−36.73	−72.46	**Present Study**	30.00	29.30	29.39	29.99	31.00	32.19	30.90
	Temuco	−38.68	−72.60		28.00	29.77	29.79	30.65	32.05	33.52	32.62
	Puerto Montt	−41.41	−72,92		31.00	30.43	30.31	31.93	33.54	35.38	35.04

CORRECTED

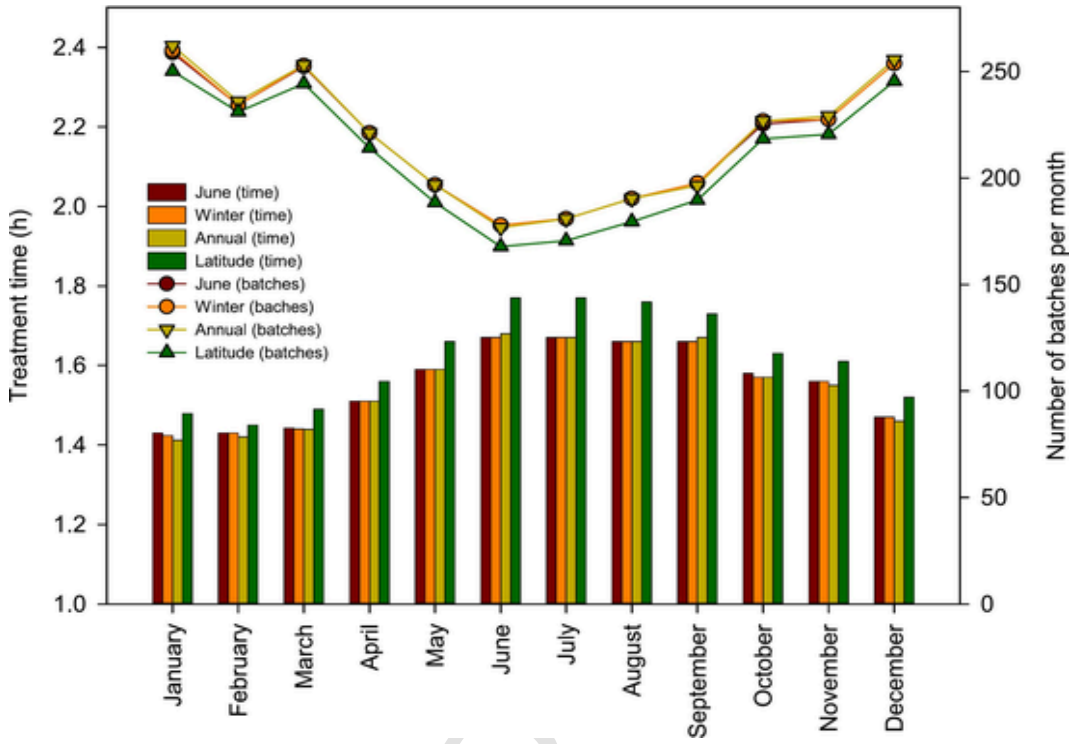

Fig. 6. Variation throughout the year in the treatment time required to decontaminate paracetamol-contaminated wastewater and the number of batches that can be processed monthly, using the optimal tilt angles for June, winter, and the entire year, as well as the tilt angle corresponding to the local latitude.

highest treatment times for each month compared to the other design options (specifically, between 0.04 and 0.07 h longer). The differences among the other three design alternatives are minimal, with slight variations that do not significantly favour any one option. In this regard, the small differences in UVR values have a reduced impact on process efficiency due to the influence of temperature, which also plays an important role. The calculation of the number of batches processed each month (available sun hours divided by treatment time, as shown in Eq. 12) follows a similar trend, though the differences between the local latitude design option and the other alternatives become more pronounced. Annually, while 2,520 batches can be processed with the local latitude tilt angle, this number increases to 2,617, 2,620, and 2,625 batches for the designs based on the optimal tilt angles for June, winter, and the entire year, respectively. Consequently, the importance of fine-tuning the photoreactor tilt angle at the local level is demonstrated, underscoring the value of developing accurate UVR models as the ones of this work.

The next step was to calculate the monthly treatment capacity (m^3 of wastewater that can be treated during a month) based on the selected tilt angle and compare it to the treatment objective (m^3 of wastewater that needs to be treated in the same month). The treatment capacity is determined by multiplying the number of batches that can be carried out by the photoreactor volume (Section 2.4). Two different methods for calculating the photoreactor volume are available, as described in the second paragraph of this section: (i) using the average annual UVR value, or (ii) using the lowest average monthly UVR value. Since the photoreactor volume also depends on the selected tilt angle, because it affects the UVR values, but the comparison of treatment capacities requires a fixed photoreactor size, the average photoreactor volume for all four options was used to calculate the data presented in Figs. 7 and 8. Consequently, the photoreactor volumes were determined to be 14.1 m^3 when using the annual UVR value and 17.4 m^3 when using the lowest average monthly UVR value.

Using the photoreactor volume based on annual averages results in scaling-up failure when the local latitude is used as the tilt angle (Fig. 7). This is the only design option where the balance between the excess treatment capacity from October to April is significantly lower than the reduced treatment capacity from May to September, leading to a wastewater treatment deficit of more than 1,000 m^3. Therefore, discarding the local latitude as a tilt angle, the focus shifts to the June, winter, and annual optimal tilt angles. While the differences between these options are not very significant, there are some noteworthy aspects. The annual balance between periods of excess and reduced treatment capacity favours the design based on the optimal annual tilt angle. In this case, 424 extra batches are available compared to 354 and 312 extra batches for the winter and June optimal tilt angles, respectively. On the other hand, when comparing the difference between the highest and lowest treatment capacities, the June optimal tilt angle is more favourable. This suggests that fluctuations in treatment capacity are slightly smoother with the June optimal tilt angle, followed by the winter optimal tilt angle, and then the annual optimal tilt angle. This would lead to a reduced need for wastewater storage during the winter period.

Using the photoreactor volume based on the lowest monthly UVR values results in a similar analysis. While no advantage can be identified in using the local latitude as the photoreactor tilt angle, the differences among the other options are not significant. However, given that no buffer tank (wastewater storage) is needed during the winter period when using this photoreactor volume, the yearly optimal tilt angle proves to be the best option. It provides an extra treatment capacity of 9,166 m^3, compared to the 9,080 m^3 and 9,028 m^3 obtained with the winter optimal tilt angle and June optimal tilt angle, respectively.

4. Limitations and future recommendation

As it was seen, the tilt angle determines the amount of UVR that the photoreactor receives, which in turn influences the amount of energy it can harvest. Therefore, finding the optimal tilt angle is essential for

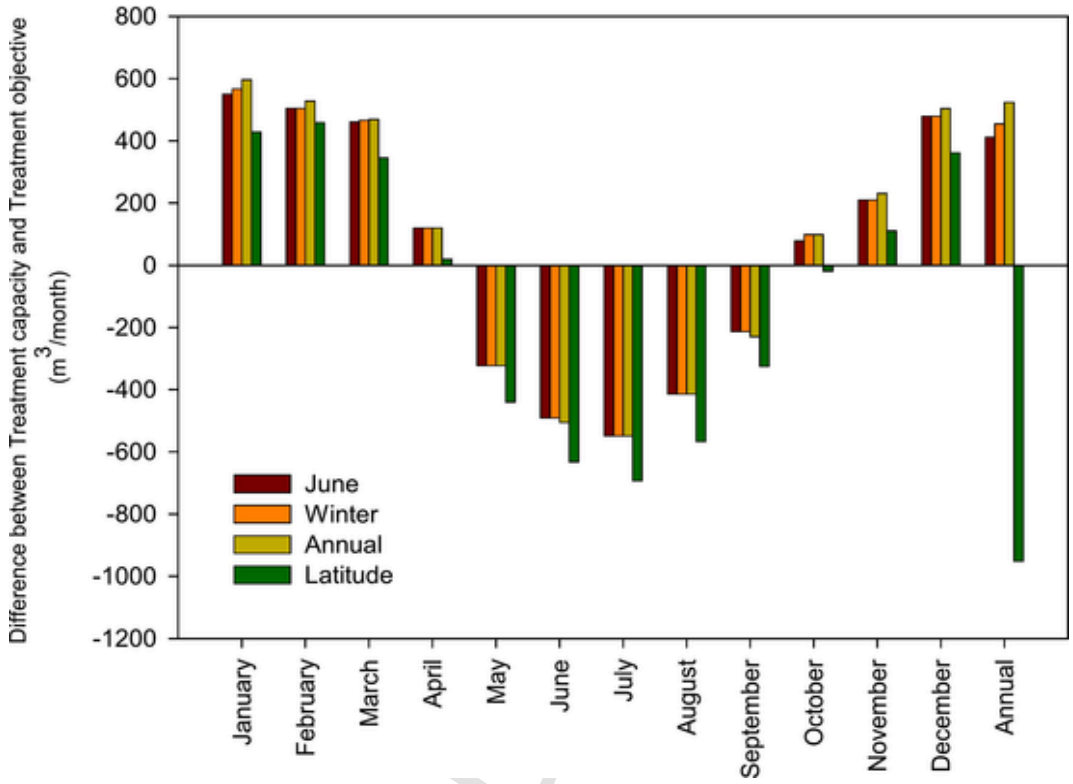

Fig. 7. Variation throughout the year in the difference between the monthly and annual treatment capacity and the objective treatment volume for the same period, using the optimal tilt angles for June, winter, and the entire year, as well as the tilt angle corresponding to the local latitude (photoreactor volume: 14.1 m^3).

maximizing the photochemical efficiency of solar photoreactors. The results of this study contribute to the existing literature on the optimal tilt angle for solar water collectors. Provides practical guidelines for installing solar-based technologies in different regions of the Southern Hemisphere. However, it is important to note that the optimal tilt angle can vary depending on other factors such as atmospheric conditions, local weather patterns, and the specific design of the solar photoreactor system which were not considered in this study and could potentially influence UVR values.

In addition, modeling UVR using isotropic models involves several limitations that can affect the accuracy of the results. For example, the assumption does not consider the variability in atmospheric conditions, such as cloud cover, aerosols, and atmospheric composition, which can significantly alter the intensity and distribution of UVR. These factors can cause spatial and temporal variations in UVR levels that isotropic models may not accurately capture. Related to this, model input data requirements may be based on simplified data inputs, which may limit their ability to incorporate detailed environmental and atmospheric data. This may result in models that are less sensitive to local variations and specific conditions. Furthermore, assume that UVR is uniformly distributed in all directions, which is a simplification that may not capture the complexities of real-world scenarios. Isotropic models fail to account for the anisotropic nature of UVR. In reality, UVR is not uniformly distributed; it is often more intense in specific directions due to factors such as the position of the sun, atmospheric conditions, and surface reflections. This can lead to inaccuracies in predicting UVR exposure, particularly in environments where directional distribution plays a significant role.

To address these limitations, more sophisticated modeling approaches, such as radiative transfer models, anisotropic models or machine learning [5,24,44], can be employed. These models incorporate detailed information about the directional distribution of UVR, atmospheric conditions, surface properties, and temporal variations, providing more accurate and realistic assessments of UVR exposure. Additionally, validation against observational measurements can help refine isotropic models and improve their reliability in specific applications. Future research could focus on developing more sophisticated models that consider other factors, such as the sun's angle [35], ground reflectivity, topography [75] or atmospheric parameters that influenced the UVR levels [52].

The result shown here assesses that the tilt angle affects the amount of light that reaches the photoreactor, influencing the rate of the solar-driven chemical reactions such as photocatalysis. For instance, it would be interesting to investigate practical strategies for adjusting tilt angles and how this could be incorporated into the design of adjustable solar photoreactor systems. For smaller-scale or budget-constrained operations, manual adjustments can be a viable strategy. This involves periodically changing the tilt angle based on the position of the sun and the specific requirements of the photoreactor. In the case of large-scale, automated tracking systems can be employed to continuously adjust the tilt angle of photoreactors to maximize light exposure throughout the day. Systems combining automated and manual strategies can also offer a balanced solution, providing some level of automation while keeping costs manageable. In this regard, it is recommended to evaluate the potential efficiency gains against the costs of implementing automated systems. In the case of large-scale operations, the increased efficiency may justify the higher costs. Also, ensure that the chosen system is reliable and that resources are available for its maintenance. Automated systems require skilled maintenance, while manual systems rely on periodic human intervention. Therefore, the strategy selection for adjusting tilt angles in photoreactors will depend on a comprehensive analysis of the specific process requirements, cost considerations, and local conditions.

CORRECTED PROOF

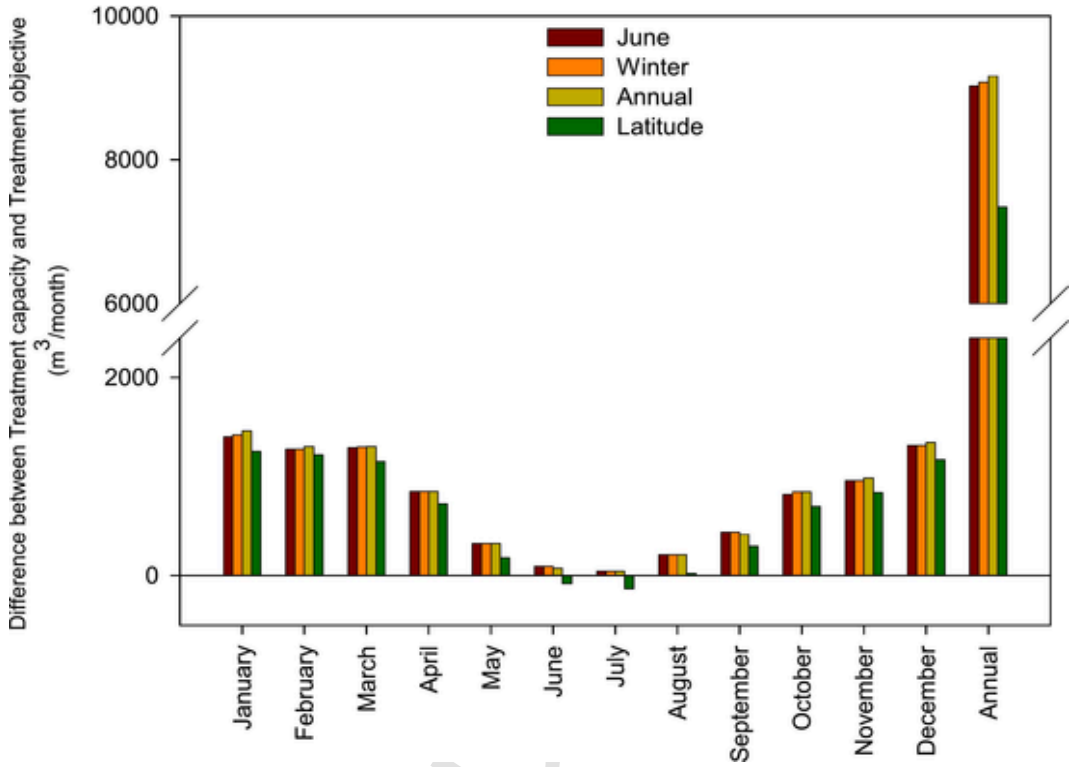

Fig. 8. Variation throughout the year in the difference between the monthly and annual treatment capacity and the objective treatment volume for the same period, using the optimal tilt angles for June, winter, and the entire year, as well as the tilt angle corresponding to the local latitude (photoreactor volume: 17.4 m^3).

Additionally, further studies could explore the impact of different solar photoreactor technologies on the optimal tilt angle. As photoreactor designs and applications become increasingly diverse [76], understanding the interplay between technology-specific characteristics and environmental factors is crucial for optimizing performance. The optimal tilt angle for a photoreactor is influenced by factors such as light capture efficiency, reactor geometry, and the specific photochemical or photobiological processes involved. For example, CPCs generally have higher light capture efficiency due to their concentrating ability, which allows them to perform well even with suboptimal tilt angles. Raceway reactors, on the other hand, benefit from maximizing surface exposure, making tilt angle adjustments more critical. CPCs offer more flexibility in terms of installation and operation due to their broad acceptance angle. Raceway reactors require more careful consideration of tilt angles to optimize light exposure and minimize shading effects. Adjusting tilt angles in CPC systems may involve more complex mechanisms due to their concentrating optics, whereas raceway reactors can be adjusted more simply but may require more frequent changes to account for seasonal variations. In this regard, studies are recommended to determine the optimal tilt angles for both CPCs and raceway reactors in different geographical locations, considering variations in solar path and intensity. In addition, explore the potential of integrating CPCs with raceway reactors to combine the benefits of concentrated light and large surface area exposure. This could involve hybrid systems that adjust tilt angles dynamically based on real-time solar conditions. By considering technology-specific characteristics, seasonal and geographical variability, and the integration of advanced tracking or manual technologies, researchers can develop innovative solutions that maximize energy conversion efficiency across different times of the year. This research not only contributes to the advancement of solar energy technologies, but also supports the broader transition to sustainable energy systems.

5. Conclusion

This research addresses a significant gap in our understanding of how to optimize UVR gains for systems water treatment (photocatalysis or solar disinfection process) in diverse geographical conditions. These findings are significant in several ways.

First, estimation of incident UVR on tilted surfaces is provided for different Chilean latitudes. This is fundamental data for the design and installation of solar systems.

Second, the research shows that the gains in UVR can be significantly increased at higher latitudes through monthly and seasonal adjustments. This suggests that the efficiency of solar water treatment systems can be improved even in regions with less optimal solar radiation conditions.

Third, the proposed correlations for calculating the optimal tilt angle are highly accurate ($R^2 \geq 0.81$, RMSE $\leq 0.98°$, MAPE ≤ 2.70,% SSRE $\leq 0.01°$, RSE $\leq 0.02°$, and MBE $\leq 0.001°$). The research has produced a series of practical models for estimating the optimal tilt angle for regions in the Southern Hemisphere, spanning from −18.44°S to −41.41°S. These models can be reliably used in academic and industrial settings to optimize the design and operation of solar water treatment systems.

Finally, the comparison of paracetamol-contaminated wastewater treatment in a CPC photoreactor with different fixed tilt angles demonstrated the importance of locally fine-tuning this inclination. According to the simulation, using the local latitude as the tilt angle (baseline) resulted in lower treatment capacities throughout the year compared to using the optimal tilt angle for the month with the lowest average UVR, for the winter period, and the entire year. This is influenced not only by UVR levels but also by operating temperature, which plays a critical role in the efficiency of the photo-Fenton process.

In conclusion, this research provides valuable insights and practical tools for optimizing the use of UVR in solar water treatment systems.

CORRECTED

These findings can be used to improve the efficiency of these systems, thereby enhancing access to clean water and contributing to sustainable development goals in Chile and other countries with similar geographical conditions.

CRediT authorship contribution statement

Lisdelys González-Rodríguez: Writing – review & editing, Writing – original draft, Visualization, Validation, Supervision, Software, Resources, Project administration, Methodology, Investigation, Formal analysis, Data curation, Conceptualization. **Basharat Jamil:** Writing – review & editing, Writing – original draft, Validation, Investigation, Formal analysis. **Mehmet Ali Kallioğlu:** Writing – review & editing, Writing – original draft, Visualization, Validation, Software, Methodology, Formal analysis, Data curation, Conceptualization. **Alejandro Cabrera-Reina:** Writing – review & editing, Visualization, Validation, Supervision, Software, Methodology, Investigation, Formal analysis, Data curation, Conceptualization. **Aitor Marzo:** Writing – review & editing, Validation, Methodology, Investigation, Formal analysis. **Wirmer García:** Writing – review & editing, Software, Methodology, Investigation, Formal analysis. **Matías Volke:** Writing – review & editing, Visualization, Validation, Methodology, Formal analysis. **Fabiola Lobos:** Writing – review & editing, Validation, Investigation, Formal analysis, Data curation. **Agustin Laguarda:** Writing – review & editing, Validation, Supervision, Methodology, Investigation, Formal analysis, Conceptualization.

Declaration of competing interest

The authors declare that they have no known competing financial interests or personal relationships that could have appeared to influence the work reported in this paper.

Acknowledgments

Lisdelys González R. thanks the competitive Fund for Regular Research Projects 2023-2024 granted by UDLA. The authors thank ANID/FONDAP/1523A0006 “Solar Energy Research Center” SERC-Chile; Chilean Economic Development Agency (CORFO) and ANID/FONDECYT/1230704. The authors also acknowledge the CACTUS project funded by the European Commission in the HORIZON-INFRA-2023-DEV-01-06 program (Ref.: 101132182). A. Marzo thanks for the Ramon y Cajal contract (RYC2021-031958-I), founded by the Spanish Ministry of Science and Innovation MCIN/AEI/10.13039/501100011033 and by the European Union “NextGenerationEU/PRTR”. SoDa Service for making solar radiation data available for public use.

References

Rivas, M., Calaf, G.M., Laroze, D., Rojas, E., Mendez, J., Honeyman, J., et al., 2020. Solar ultraviolet A radiation and nonmelanoma skin cancer in Arica Chile. J. Photochem. Photobiol. B 212, 112047. https://doi.org/10.1016/j.jphotobiol.2020.112047.

Lofrano, G., Libralato, G., Casaburi, A., Siciliano, A., Iannece, P., Guida, M., et al., 2018. Municipal wastewater spiramycin removal by conventional treatments and heterogeneous photocatalysis. Sci. Total Environ. 624, 461–469. https://doi.org/10.1016/j.scitotenv.2017.12.145.

Cabrera-Reina, A., Miralles-Cuevas, S., Soriano-Molina, P., Sánchez-Pérez, J.A., 2021. A critical evaluation of the use of accumulated energy as a parameter for the scale-up of solar photoreactors during the treatment of simulated industrial wastewater by solar photo-Fenton. J. Chem. Technol. Biotechnol. 96, 1593–1602. https://doi.org/10.1002/jctb.6678.

Kant, P., Liang, S., Rubin, M., Ozin, G.A., Dittmeyer, R., 2023. Low-cost photoreactors for highly photon/energy-efficient solar-driven synthesis. Joule 7, 1347–1362. https://doi.org/10.1016/j.joule.2023.05.006.

González-Rodríguez, L., Cabrera-Reina, A., Rosas, J., Volke, M., Marzo, A., 2024. Characterization of solar-derivate ultraviolet radiation for water solar treatment applications. Renew. Energy 233. https://doi.org/10.1016/j.renene.2024.121078.

Jacobson, M.Z., 1999. Isolating nitrated and aromatic aerosols and nitrated aromatic gases as sources of ultraviolet light absorption. J. Geophys. Res. Atmos. 104, 3527–3542. https://doi.org/10.1029/1998JD100054.

Escobedo, J.F., Gomes, E.N., Oliveira, A.P., Soares, J., 2009. Modeling hourly and daily fractions of UV, PAR and NIR to global solar radiation under various sky conditions at Botucatu Brazil. Appl Energy 86, 299–309. https://doi.org/10.1016/j.apenergy.2008.04.013.

Delcourt, C., Cougnard-Grégoire, A., Boniol, M., Carrière, I., Doré, J.F., Delyfer, M.N., et al., 2014. Lifetime exposure to ambient ultraviolet radiation and the risk for cataract extraction and age-related macular degeneration: the alienor study. Invest. Ophthalmol. Vis. Sci. 55, 7619–7627. https://doi.org/10.1167/iovs.14-14471.

González-Rodríguez, L., Jiménez, J., Rodríguez-López, L., de Oliveira, A.P., Baeza, A.C., Contreras, D., et al., 2021. Ultraviolet erythemal radiation in Central Chile: direct and indirect implication for public health. Air Qual. Atmos. Health 14, 1533–1548. https://doi.org/10.1007/s11869-021-01037-3.

Castro-alférez, M., Polo-lópez, M.I., Marugán, J., 2018. Validation of a solar-thermal water disinfection model for Escherichia coli inactivation in pilot scale solar reactors and real conditions. Chem. Eng. J. 331, 831–840. https://doi.org/10.1016/j.cej.2017.09.015.

Figueredo-Fernández, M., Gutiérrez-alfaro, S., Acevedo-merino, A., Manzano, M.A., 2017. Estimating lethal dose of solar radiation for enterococcus inactivation through radiation reaching the water layer. application to Solar Water Disinfection (SODIS). Sol. Energy 158, 303–310. https://doi.org/10.1016/j.solener.2017.09.006.

Blanco, J., Malato, S., Fernández-Ibañez, P., Alarcón, D., Gernjak, W., Maldonado, M.I., 2009. Review of feasible solar energy applications to water processes. Renew. Sustain. Energy Rev. 13, 1437–1445. https://doi.org/10.1016/j.rser.2008.08.016.

Malato, S., Maldonado, M.I., Fernández-ibáñez, P., Oller, I., Polo, I., Sánchez-moreno, R., 2016. Decontamination and disinfection of water by solar photocatalysis: the pilot plants of the Plataforma Solar de Almeria. Mater. Sci. Semicond. Process. 42, 15–23. https://doi.org/10.1016/j.mssp.2015.07.017.

García-gil, Á., Valverde, R., García-muñoz, R.A., Mcguigan, K.G., Marugán, J., 2020. Solar water disinfection in high-volume containers: are naturally occurring substances attenuating factors of radiation? Chem. Eng. J. 399, 125852. https://doi.org/10.1016/j.cej.2020.125852.

Lu, H., Fan, W., Dong, H., Liu, L., 2017. Dependence of the irradiation conditions and crystalline phases of TiO2 nanoparticles on their toxicity to Daphnia magna. Environ. Sci. Nano 4, 406–414. https://doi.org/10.1039/c6en00391e.

Cabrera Reina, A., Miralles-Cuevas, S., Cornejo, L., Pomares, L., Polo, J., Oller, I., et al., 2020. The influence of location on solar photo-Fenton: process performance, photoreactor scaling-up and treatment cost. Renew. Energy 145, 1890–1900. https://doi.org/10.1016/j.renene.2019.07.113.

Herrmann, J.M., 1999. Heterogeneous photocatalysis: fundamentals and applications to the removal of various types of aqueous pollutants. Catal. Today 53, 115–129. https://doi.org/10.1016/S0920-5861(99)00107-8.

Despotovic, M., Nedic, V., 2015. Comparison of optimum tilt angles of solar collectors determined at yearly, seasonal and monthly levels. Energy Convers Manag 97, 121–131. https://doi.org/10.1016/j.enconman.2015.03.054.

Abdallah, R., Juaidi, A., Abdel-Fattah, S., Manzano-Agugliaro, F., 2020. Estimating the optimum tilt angles for south-facing surfaces in Palestine. Energies (Basel) 13. https://doi.org/10.3390/en13030623.

Chong, M.N., Jin, B., Chow, C.W.K., Saint, C., 2010. Recent developments in photocatalytic water treatment technology: a review. Water Res. 44, 2997–3027. https://doi.org/10.1016/j.watres.2010.02.039.

Malato, S., Fernández-Ibáñez, P., Maldonado, M.I., Blanco, J., Gernjak, W., 2009. Decontamination and disinfection of water by solar photocatalysis: Recent overview and trends. Catal. Today 147, 1–59. https://doi.org/10.1016/j.cattod.2009.06.018.

Klotz, B., Gradl, R., Schenzinger, V., Schwarzmann, M., Schreder, J., Lorenz, S., et al., 2025. UV map nowcasting and comparison with ground-based UV measurements for the DACH region. Remote Sens. (Basel) 17, 629. https://doi.org/10.3390/rs17040629.

Shukla, K.N., Rangnekar, S., Sudhakar, K., 2015. Comparative study of isotropic and anisotropic sky models to estimate solar radiation incident on tilted surface: a case study for Bhopal India. Energy Reports 1, 96–103. https://doi.org/10.1016/j.egyr.2015.03.003.

Qadeer, A., Parvez, M., Khan, O., Jafri, H.Z., Lal, S., 2024. Optimization of solar radiation on tilted surface in isotropic and anisotropic atmospheric conditions. Next Research 1, 100075. https://doi.org/10.1016/j.nexres.2024.100075.

Maleki, S.A.M., Hizam, H., Gomes, C., 2017. Estimation of hourly, daily and monthly global solar radiation on inclined surfaces: models re-visited. Energies (Basel) 10. https://doi.org/10.3390/en10010134.

Utrillas, M.P., Marín, M.J., Esteve, A.R., Estellé, V., Tena, F., Cañ Ada, J., et al., 2009. Diffuse ultraviolet erythemal irradiance on inclined planes: a comparison of experimental and modeled data. Photochem. Photobiol. 85, 1245–1253. https://doi.org/10.1111/j.1751-1097.2009.00573.x.

Gueymard, C.A., 2019. The SMARTS spectral irradiance model after 25years: new developments and validation of reference spectra. Sol. Energy 187, 233–253. https://doi.org/10.1016/j.solener.2019.05.048.

Sandmann, H., Stick, C., 2014. Spectral and spatial UV sky radiance measurements at a seaside resort under clear sky and slightly overcast conditions. Photochem. Photobiol. 90, 225–232. https://doi.org/10.1111/php.12180.

R.H. Grant, G.M. Heisler, W. Gao, Theoretical and Applied Climatorogy Clear Sky Radiance Distributions in Ultraviolet Wavelength Bands. vol. 56. 1997.

Jamil, B., Siddiqui, A.T., Akhtar, N., 2016. Estimation of solar radiation and optimum tilt angles for south-facing surfaces in Humid Subtropical Climatic Region of India. Engineering Science and Technology, an International Journal 19, 1826–1835. https://doi.org/10.1016/j.jestch.2016.10.004.

Jafarkazemi, F., Saadabadi, S.A., 2013. Optimum tilt angle and orientation of solar surfaces in Abu Dhabi UAE. Renew. Energy 56, 44–49. https://doi.org/10.1016/j.renene.2012.10.036.

CORRECTED PROOF

H. Ghedira, Y. Eissa, Global tilt irradiation map of the United Arab Emirates. Energy Procedia, vol. 57, Elsevier Ltd; 2014, p. 1199–205. Doi: 10.1016/j.egypro.2014.10.107.
Navntoft, L.C., Fernandez-Ibañez, P., Garreta, F., 2012. UV solar radiation on a tilted and horizontal plane: analysis and comparison of 4years of measurements. Sol. Energy 86, 307–318. https://doi.org/10.1016/j.solener.2011.10.004.
Aksoy Tırmıkçı, C., Yavuz, C., 2018. Determining optimum tilt angles of solar surfaces in Sakarya Turkey. Theor Appl Climatol 133, 15–22. https://doi.org/10.1007/s00704-017-2174-x.
Kallioğlu, M.A., Durmuş, A., Karakaya, H., Yılmaz, A., 2020. Empirical calculation of the optimal tilt angle for solar collectors in northern hemisphere. Energy Sources Part A 42, 1335–1358. https://doi.org/10.1080/15567036.2019.1663315.
Kaddoura, T.O., Ramli, M.A.M., Al-Turki, Y.A., 2016. On the estimation of the optimum tilt angle of PV panel in Saudi Arabia. Renew. Sustain. Energy Rev. 65, 626–634. https://doi.org/10.1016/j.rser.2016.07.032.
Alqaed, S., Mustafa, J., Almehmadi, F.A., Jamil, B., 2023. Estimation of ideal tilt angle for solar-PV panel surfaces facing south: a case study for Najran City Saudi Arabia. J. Therm. Anal. Calorim. 148, 8641–8654. https://doi.org/10.1007/s10973-022-11812-8.
Uba, F.A., Sarsah, E.A., 2013. Optimization of tilt angle for solar collectors in WA, Ghana. Pelagia Research Library Advances in Applied Science Research 4, 108–114.
Cronemberger, J., Caamaño-Martín, E., Sánchez, S.V., 2012. Assessing the solar irradiation potential for solar photovoltaic applications in buildings at low latitudes - making the case for Brazil. Energ. Buildings 55, 264–272. https://doi.org/10.1016/j.enbuild.2012.08.044.
González-Rodríguez, L., Pérez, L., Fissore, A., Rodríguez-López, L., Jimenez, J., 2019. In: Tilt and Orientation of a Flat Solar Collector to Capture Optimal Solar Irradiation in Chilean Latitudes. Springer International Publishing, pp. 215–228. https://doi.org/10.1007/978-3-030-04233-2_19.
Yadav, A.K., Chandel, S.S., 2013. Tilt angle optimization to maximize incident solar radiation: a review. Renew. Sustain. Energy Rev. 23, 503–513. https://doi.org/10.1016/j.rser.2013.02.027.
Jacobson, M.Z., Jadhav, V., 2018. World estimates of PV optimal tilt angles and ratios of sunlight incident upon tilted and tracked PV panels relative to horizontal panels. Sol. Energy 169, 55–66. https://doi.org/10.1016/j.solener.2018.04.030.
Chinchilla, M., Santos-Martín, D., Carpintero-Rentería, M., Lemon, S., 2021. Worldwide annual optimum tilt angle model for solar collectors and photovoltaic systems in the absence of site meteorological data. Appl. Energy 281. https://doi.org/10.1016/j.apenergy.2020.116056.
Rinchi, B., Dababseh, R., Jubran, M., Al-Dahidi, S., Abdalla, M.E.B., Ayadi, O., 2025. Global prediction of optimal solar panel tilt angles via machine learning. Appl. Energy 382. https://doi.org/10.1016/j.apenergy.2025.125322.
Serrano, 2010. Measurement and modelling of global erythemal irradiance on inclined planes. Tethys, Journal of Weather and Climate of the Western Mediterranean. https://doi.org/10.3369/tethys.2010.7.05.
C. Burattini, M. Borra, F. Vespasiano, F. Bisegna, UV Solar Energy and Erythemal Exposure: Mathematical Models to Assess the Dose on Vertical and Inclined Planes in Different Sky Conditions. Energies (Basel) 2024;17. Doi: 10.3390/en17225718.
Serrano, D., Marín, M.J., Utrillas, M.P., Tena, F., Martínez-Lozano, J.A., 2012. Modelling of the UV Index on vertical and 40° tilted planes for different orientations. Photochem. Photobiol. Sci. 11, 333–344. https://doi.org/10.1039/c1 pp05211j.
Palma, G., Śnchez, A., Olave, Y., Encina, F., Palma, R., Barra, R., 2004. Pesticide levels in surface waters in an agricultural-forestry basin in Southern Chile. Chemosphere 57, 763–770. https://doi.org/10.1016/j.chemosphere.2004.08.047.
Cooman, K., Debels, P., Gajardo, M., Urrutia, R., Barra, R., 2005. Use of Daphnia spp. for the ecotoxicological assessment of water quality in an agricultural watershed in South-Central Chile. Arch. Environ. Contam. Toxicol. 48, 191–200. https://doi.org/10.1007/s00244-004-0218-6.
Climent, M.J., Herrero-Hernández, E., Sánchez-Martín, M.J., Rodríguez-Cruz, M.S., Pedreros, P., Urrutia, R., 2019. Residues of pesticides and some metabolites in dissolved and particulate phase in surface stream water of Cachapoal River basin, central Chile. Environ. Pollut. 251, 90–101. https://doi.org/10.1016/j.envpol.2019.04.117.
Cordero, R.R., Roth, P., Georgiev, A., Dasilva, L., 2005. Climatology of surface ultraviolet-radiation in Valparaiso Chile. Energy Convers Manag 46, 2907–2918. https://doi.org/10.1016/j.enconman.2005.02.008.
González-Rodríguez, L., Lien, R., López, R., Jiménez, J., Rosas, J., García, W., 2022. Spatio – temporal estimations of ultraviolet erythemal radiation in Central Chile. Air Qual. Atmos. Health. https://doi.org/10.1007/s11869-022-01195-y.
Gschwind, M.L., Albuisson, M., Wald, L., 2006. Converting a successful research project into a sustainable service: the case of the SoDa Web service. Enviromental Modelling & Software 21, 1555–1561. https://doi.org/10.1016/j.envsoft.2006.05.002.
A. Aculinin, C. Brogniez, M. Bengulescu, D. Gillotay, F. Auriol, L. Wald, Assessment of several empirical relationships for deriving daily means of UV-A irradiance from meteosat-based estimates of the total irradiance. Remote Sens (Basel) 2016;8. Doi: 10.3390/rs8070537.
Gašparović, I., Gašparović, M., Medak, D., 2018. Determining and analysing solar irradiation based on freely available data: a case study from Croatia. Environ. Dev. 26, 55–67. https://doi.org/10.1016/j.envdev.2018.04.001.
Wahab, M.A., El-Metwally, M., Hassan, R., Lefévre, M., Oumbe, A., Wald, L., 2010. Assessing surface solar irradiance and its long-term variations in the northern Africa desert climate using Meteosat images. Int. J. Remote Sens. 31, 261–280. https://doi.org/10.1080/01431160902882645.
Engerer, N.A., 2015. Minute resolution estimates of the diffuse fraction of global irradiance for southeastern Australia. Sol. Energy 116, 215–237. https://doi.org/10.1016/j.solener.2015.04.012.
L. Wald, Elements on the computation of UV maps in the Eurosun database. 2012.
Cotfas, D.T., Cotfas, P.A., Kaplani, E., Samoila, C., 2014. Monthly average daily global and diffuse solar radiation based on sunshine duration and clearness index for Brasov, Romania. J. Renewable Sustainable Energy 6. https://doi.org/10.1063/1.4896596.
Hagihara, Y., Okamoto, H., Yoshida, R., 2010. Development of a combined CloudSat-CALIPSO cloud mask to show global cloud distribution. J. Geophys. Res. Atmos. 115, 1–17. https://doi.org/10.1029/2009JD012344.
Winker, D.M., Pelon, J., 2003. The CALIPSO mission. International Geoscience and Remote Sensing Symposium (IGARSS) 2, 1329–1331. https://doi.org/10.1175/2010bams3009.1.
Liu, B.Y., Jordan, R., 1961. Daily insolation on surfaces tilted towards equator. ASHRAE J. 10.
Despotovic, M., Nedic, V., Despotovic, D., Cvetanovic, S., 2016. Evaluation of empirical models for predicting monthly mean horizontal diffuse solar radiation. Renew. Sustain. Energy Rev. 56, 246–260. https://doi.org/10.1016/j.rser.2015.11.058.
Cabrera Reina, A., Casas López, J.L., Maldonado Rubio, M.I., Santos-Juanes Jordá, L., García Sánchez, J.L., Sánchez Pérez, J.A., 2014. Effects of environmental variables on the photo-Fenton plant design. Chem. Eng. J. 237, 469–477. https://doi.org/10.1016/j.cej.2013.10.046.
Farias, J., Albizzati, E.D., Alfano, O.M., 2009. Kinetic study of the photo-Fenton degradation of formic acid. combined effects of temperature and iron concentration. Catal. Today 144, 117–123. https://doi.org/10.1016/j.cattod.2008.12.027.
Zapata, A., Oller, I., Rizzo, L., Hilgert, S., Maldonado, M.I., Sánchez-Pérez, J.A., et al., 2010. Evaluation of operating parameters involved in solar photo-Fenton treatment of wastewater: Interdependence of initial pollutant concentration, temperature and iron concentration. Appl Catal B 97, 292–298. https://doi.org/10.1016/j.apcatb.2010.04.020.
Marzo, A., Salmon, A., Polo, J., Ballestrín, J., Soto, G., Quiñones, G., et al., 2021. Solar extinction map in Chile for applications in solar power tower plants, comparison with other places from sunbelt and impact on LCOE. Renew. Energy 170, 197–211. https://doi.org/10.1016/j.renene.2021.01.126.
Ferrada, P., Marzo, A., Cabrera, E., Chu, H., del Campo, V., Rabanal, J., et al., 2017. Potential for photogenerated current for silicon based photovoltaic modules in the Atacama Desert. Sol. Energy 144, 580–593. https://doi.org/10.1016/j.solener.2017.01.053.
Chapra, S.C., Canale, R.P., 2015. Numerical methods for engineers. McGraw-Hill Education.
Le Roux, W.G., 2016. Optimum tilt and azimuth angles for fixed solar collectors in South Africa using measured data. Renew. Energy 96, 603–612. https://doi.org/10.1016/j.renene.2016.05.003.
Talebizadeh, P., Mehrabian, M.A., Abdolzadeh, M., 2011. Determination of optimum slope angles of solar collectors based on new correlations. Energy Sources Part A 33, 1567–1580. https://doi.org/10.1080/15567036.2010.551253.
Santos-Martin, D., Lemon, S., 2015. SoL - a PV generation model for grid integration analysis in distribution networks. Sol. Energy 120, 549–564. https://doi.org/10.1016/j.solener.2015.07.052.
Yan, R., Saha, T.K., Meredith, P., Goodwin, S., 2013. Analysis of yearlong performance of differently tilted photovoltaic systems in Brisbane Australia. Energy Convers Manag 74, 102–108. https://doi.org/10.1016/j.enconman.2013.05.007.
J. Blanco-Gálvez, El reactor solar fotocatalítico. Solar Safe Water. ByToner, España: 2005, p. 277–83.
Weihs, P., 2002. Influence of ground reflectivity and topography on erythemal UV radiation on inclined planes. Int. J. Biometeorol. 46, 95–104. https://doi.org/10.1007/s00484-002-0124-4.
Mei, J., Gao, X., Zou, J., Pang, F., 2023. Research on photocatalytic wastewater treatment reactors: design, optimization, and evaluation criteria. Catalysts 13. https://doi.org/10.3390/catal13060974.

CORRECTED PROOF